The creation of a quasiparticle with energy E_a above the quasiparticle vacuum $|0\rangle$ is given by $A_\alpha^+|0\rangle$. This is illustrated on the far left of the figure. The transformation Eq.(3.2) from single particle states to quasiparticle energies is shown schematically in the boxed [ ] area. Finally we note that at $\varepsilon_a=\lambda$, one has $E_a=\Delta_a$; thus the correspondence between the single particle levels and the quasiparticle spectrum is shown by the connecting arrow between the sets of levels A and B.

The ground state of an even A nucleus is represented by the quasiparticle vacuum. It assumes that all particles are coupled to zero angular momentum. The excited states in such a nucleus are formed by creating 2,4,... quasiparticle excitations above the vacuum. Consequently an energy gap of at least $2\Delta_a$ develops between the ground and lowest excited state. On the other hand, an odd-A nucleus has a single quasiparticle state as its ground state. The excited states are now formed by creating either one or three, etc., quasiparticle states. There is no energy gap here as in the even-A systems, since the excited single quasiparticle levels can lie arbitrarily close to the ground state.

We note in passing, that since pairing leads to non-conservation of particle number, there must also be an

associated fluctuation in isospin [La 64]. The importance of this effect is measured by the fluctuations in isospin measured relative to its average value in the quasiparticle ground state. If $\langle T^2\rangle - \langle T\rangle^2 \ll \langle T\rangle^2$, the consequences of isospin-breaking due to pairing are small. We therefore neglect such effects in the Sn isotopes, for which the above inequality is well satisfied. For lighter systems where this neglect is less justifiable, appeal could be made to the procedures of Weneser [We 69] for discussing this problem.

3.2 EFFECT OF PAIRING ON THE SELF-ENERGY

To examine the effect of pairing on our expression for the self-energy $\Sigma_1^d(\omega)$, consider once again the Feynman representation

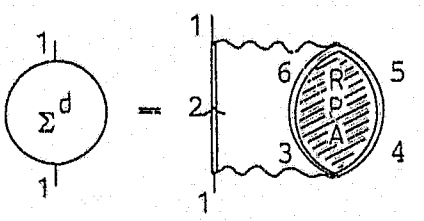

As an example, suppose the states 1,2 represent a neutron hole. The neat categorisation of nucleon states as belonging to core or valence regions that was introduced in discussing isospin is again very useful in discussing the pairing problem. If 2 falls in the core region, there are no pairing effects, and so the Green's function $G_2^b(\omega-\omega')$ necessary for the construction of $\Sigma_1^d(\omega)$ remains unchanged. However, if the state 2 belongs to the neutron valence shell, the structure of $G_2^b(\omega-\omega')$ and hence $\Sigma_1^d(\omega)$ is changed. We see this by looking at the non-interacting Green's function $iG_2^{(0)}(\omega) = \int dt\, e^{i\omega t}\langle 0|Tc_2(t)c_2^+(0)|0\rangle$. Upon inserting $c_2(t)$ and $c_2^+(0)$ in terms of the quasiparticle operators $A_2(t)=e^{-iE_2t}A_2(0)$ and $A_2^+(t)=e^{iE_2t}A_2^+(0)$, one obtains

$$G_2^{(0)}(\omega) = \left[\frac{v_2^2}{\omega+E_2-i\eta} + \frac{u_2^2}{\omega-E_2+i\eta}\right] \tag{3.5}$$

By comparison with Eq.(2.9), this expression indicates that the effect of pairing is to reduce the component

of the Green's function associated with a HF particle state 2, from unity to u_2^2, and that associated with a HF hole state from unity to v_2^2. The two terms are no longer mutually exclusive, and hence the HF propagator $G_2^{(0)}(\omega)$ clearly describes a pairing quasiparticle. This feature can be transferred to the description of $G_2^b(\omega-\omega')$, by reducing the amplitudes $|\overline{(c_2)_{s'o}}|^2$ and $|\overline{(c_2^+)_{so}}|^2$, in Eq.(2.29) by v_2^2 and u_2^2 respectively. These then become

$$\frac{\pi}{\dot{D}_{s'}} |\overline{(c_2)_{s'o}}|^2 = \frac{v_2^2 \, W_2(\lambda-\varepsilon_{s'})}{(\varepsilon_{s'}+\varepsilon_2-\lambda)^2+W_2^2(\lambda-\varepsilon_{s'})}$$

$$\text{and } \frac{\pi}{D_s} |\overline{(c_2^+)_{so}}|^2 = \frac{u_2^2 \, \dot{W}_2(\varepsilon_s+\lambda)}{(\varepsilon_s-\varepsilon_2+\lambda)^2+W_2^2(\varepsilon_s+\lambda)} \qquad (3.6)$$

and the sum rule $\sum_s |(c_2^+)_{so}|^2 + \sum_{s'} |(c_2)_{s'o}|^2 = 1$ is still satisfied. Schematically the pairing quasiparticle cannot be assigned a particle or hole character (in the sense of a Goldstone diagram). Rather we associate a non-directional unmarked line with the quasiparticle propagator as follows:

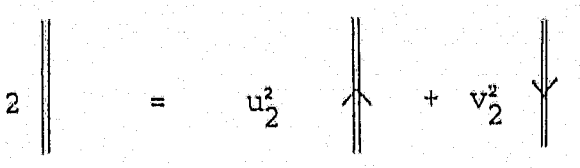

In the event that the polarization insertion on 2, either in its single bubble or RPA version, consists of <u>proton</u> core excitations the same procedures for evaluating $\Sigma_1^d(\omega)$, from either Eq.(2.41) or Eq.(2.84)

follow as before. Note however, that one may not split up any calculations into particle or hole states as was done in the evaluation of Eq.(2.84). Hence the description of a neutron (pairing) quasiparticle "stirring up" proton particle-hole excitations is given by the expression

$$\Sigma_1^d(\omega) = \sum_{Re\omega_\lambda>0} \sum_{2,J} \left(\frac{2J+1}{2j_1+1}\right) \left\{ \frac{A^J_{12,\lambda}(\omega-(\lambda+\tilde{E}_2))u_2^2}{\omega-(\lambda+\tilde{E}_2)-\omega_\lambda(\omega-(\lambda+\tilde{E}_2))+iW_2(\omega-\alpha_\lambda)} + \frac{B^J_{12,\lambda}(\lambda-\tilde{E}_2-\omega)v_2^2}{\omega-(\lambda-\tilde{E}_2)+\omega_\lambda(\lambda-\tilde{E}_2-\omega)-iW_2(\omega+\alpha_\lambda')} \right\} \tag{3.7}$$

Here we have introduced the symbol $\tilde{E}_2=(E_2-\Delta)>0$ to denote that the energy of the quasiparticle 2 is measured from Δ. $A^J_{12,\lambda}$ and $B^J_{12,\lambda}$ are as given by Eq.(2.117). This expression can be simply obtained from Eq.(2.117) by the replacement of $\varepsilon_2>\lambda$ in the first term by $\lambda+\tilde{E}_2>\lambda$, which is thus particle-like, and $\varepsilon_2<\lambda$ in the second term by $\lambda-\tilde{E}_2<\lambda$, which is hole-like. The factors $1-n_2$ and n_2 are replaced by the amplitudes u_2^2 and v_2^2 respectively. Clearly, this formula is a generalisation of Eq.(2.117) for pairing quasiparticle states, to which it reverts when $u_2^2\to 1-n_2$, $v_2^2\to n_2$, and $\tilde{E}_2\to(\varepsilon_2-\lambda)$ or $(\lambda-\varepsilon_2)$.

In the event that the RPA bubble that dresses state 2 consists of neutron excitations in the valence shell, pairing effects enter the problem in an essential way. The calculation of the associated polarisation propagator has been dealt with by Baranger [Ba 60].

3.3 APPLICATION TO THE TIN ISOTOPES

In this section, we apply these ideas to a calculation of the strength function for the isotopes of Sn. The ingredients required for such a calculation are (a) a specification of the HF single particle energies ε_1 and the quasiparticle spectrum resulting from these in a given isotope, and (b) a specification of the self-energy insertions $\Sigma_1^b(\omega)$ and $\Sigma_1^d(\omega)$ that arise from the dressing of the state 1, due to its interaction with the background directly, and via selected doorway states, respectively. Let us illustrate the implementation of these facets of the problem by describing in detail the calculation of the $g_{9/2}$ strength function that is produced by removing a neutron from ^{116}Sn.

(a) <u>The single particle energies and quasiparticle spectrum resulting from these</u>.

The shell model single particle valence levels that are relevant for discussing the nuclear structure in the vicinity of the Sn isotopes have been taken from Kisslinger and Sorensen [Ki 60] , and are shown in Fig. 3.3. The associated quasiparticle levels calculated from these are shown on the right using the common gap parameter Δ= 0.92 MeV, and the chemical potential λ=1.43 MeV measured relative to the $2d_{5/2}$ state, as calculated by Kisslinger.

The neutron threshold (zero energy point) has been located by identifying the $3s_{1/2}$ quasiparticle state with the neutron separation energy in ^{116}Sn.

Fig 3.3 Single particle levels as given by Kisslinger (ie. located relative to the $2d_{5/2}$ state) are shown, together with the associated quasiparticle spectrum. Relocation of zero is done by positioning the ground state of ^{115}Sn, i.e. the lowest quasiparticle state, at the neutron separation energy of ^{116}Sn. All energies are measured in MeV.

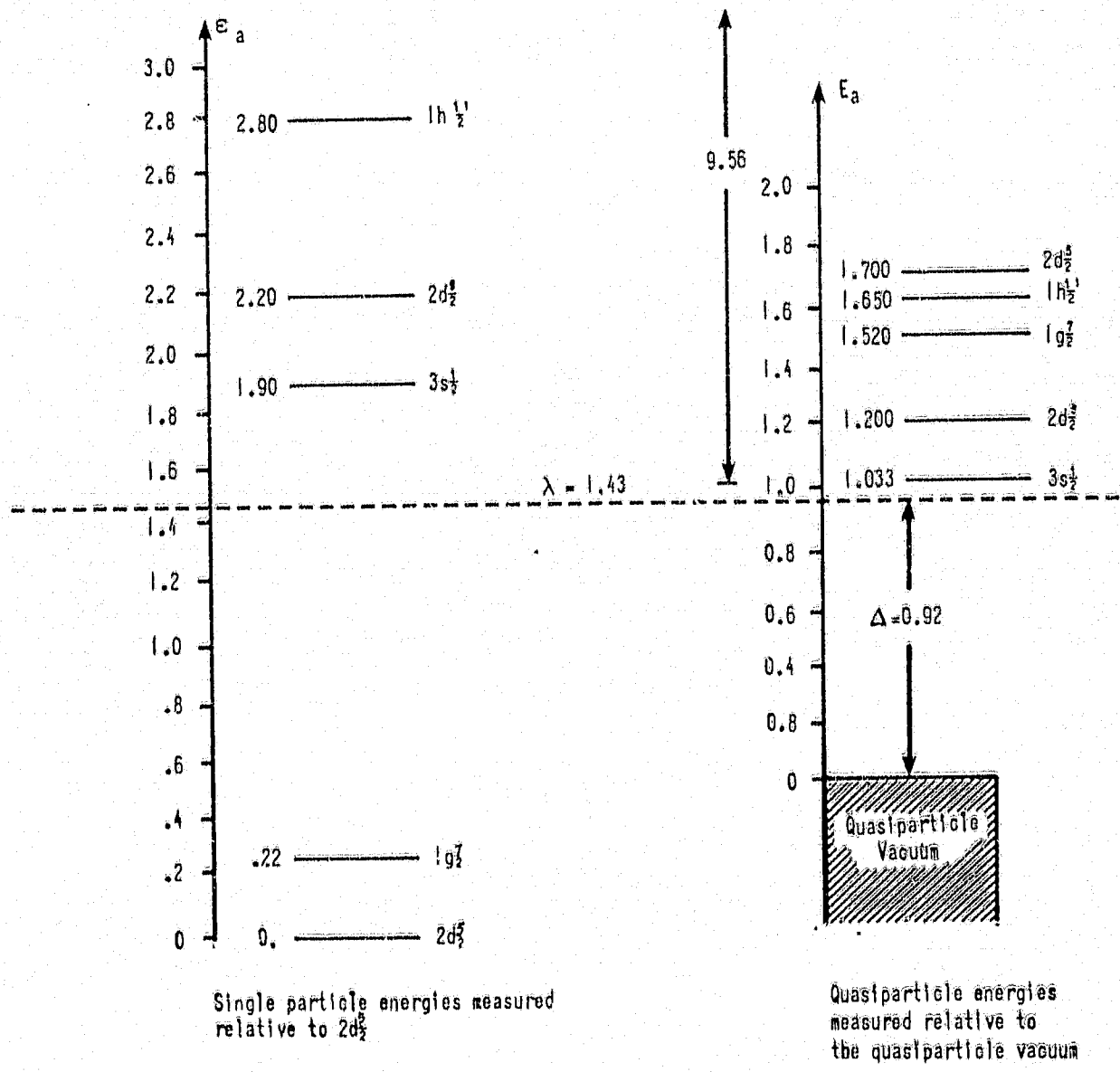

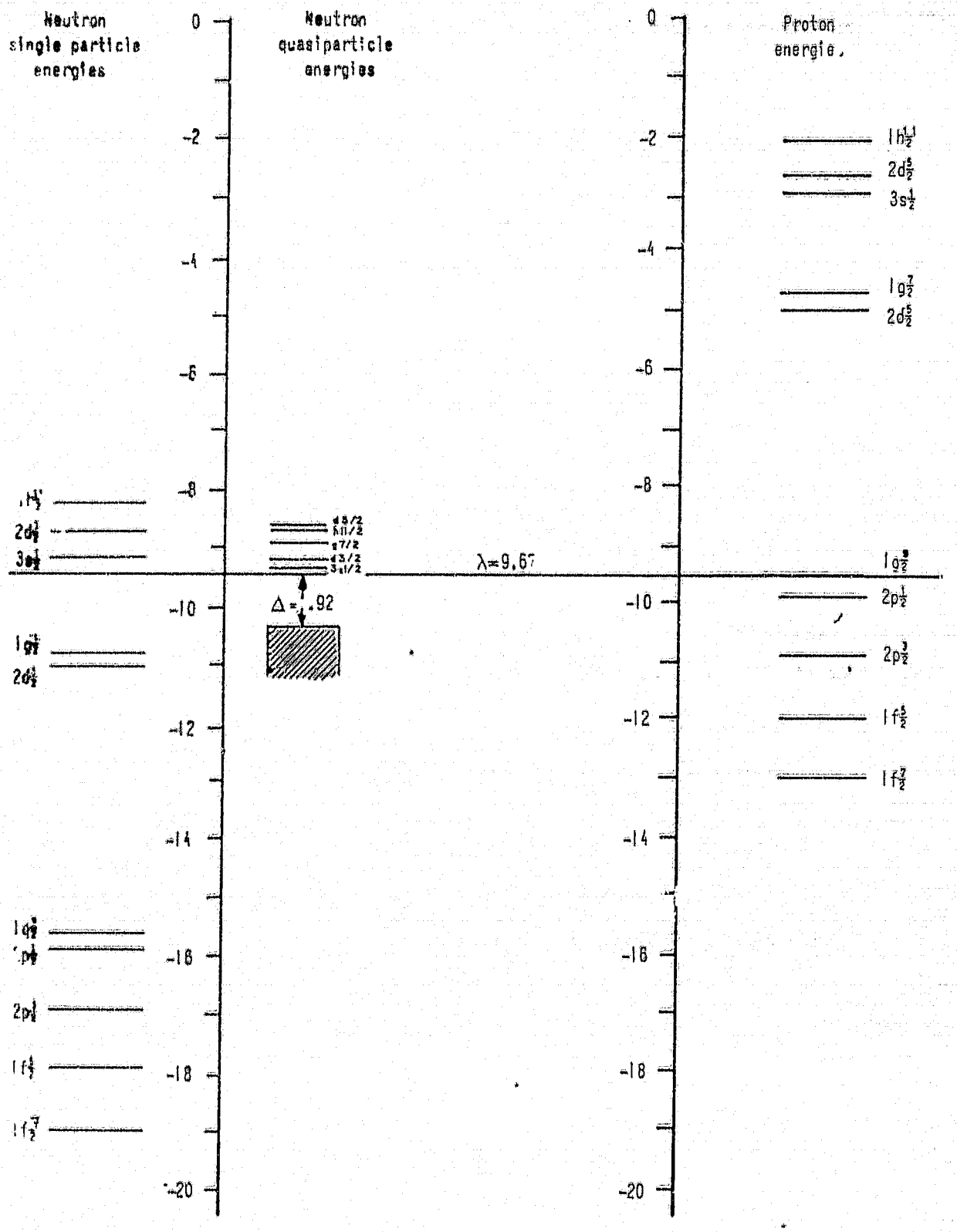

Fig 3.4 : See caption on following page.

The filled $g_{9/2}$ to $f_{5/2}$ states do not enter the pairing calculation of Kisslinger and Sorensen. We have taken the location of these from estimates of Gerlic. The proton single particle levels have been simply obtained from these by shifting the last occupied level, the $g_{9/2}$ state to the common chemical potential λ. The accuracy with which single particle energies are known does not warrant a more detailed calculation. The full single particle spectrum assumed for our problem is given in Fig. (3.4).

Fig 3.4 The neutron single particle energies relevant for ^{115}Sn are depicted on the left, relocated relative to the ground state of the target nucleus, ^{116}Sn (zero energy). The proton energies derive from these by merely shifting the $g_{9/2}$ state to λ are shown on the right. In the centre are the neutron quasiparticle energies.

This information, together with the occupation probabilities, is repeated in Tables 3.1 and 3.2.

Table 3.1 The neutron spectrum. The single particle energies, measured from the zero (neutron threshold) and as excitation energies from λ are given for the valence shell levels and first harmonic oscillator shell levels below this. The occupation probabilities v_a^2 and quasiparticle energies associated with the valence shell are also listed. These have simply been extended into the core region, by setting $v_a^2=1$, and $\tilde{E}_a=|\varepsilon_a-\lambda|$. The $3s_{1/2}$ quasiparticle lies at excitation energy 0.11 MeV from λ and hence λ lies at $-(0.11 + S_n) = -9.67$ MeV, where S_n is the neutron separation energy in ^{116}Sn.

Level	ε_a (MeV)	$(\varepsilon_a-\lambda)$ (MeV)	E_a (MeV)	$\tilde{E}_a=E_a-\Delta$ (MeV)	v_a^2
$1h_{11/2}$	- 8.30	1.37	1.65	0.73	0.09
$2d_{3/2}$	- 8.90	0.77	1.20	0.28	0.18
$3s_{1/2}$	- 9.20	0.47	1.03	0.11	0.27
$1g_{7/2}$	-10.88	1.21	1.52	0.60	0.90
$2d_{5/2}$	-11.10	1.43	1.70	0.78	0.92
$1g_{9/2}$	-15.71	6.04		6.04	1
$2p_{1/2}$	-16.01	6.34		6.34	1
$2p_{3/2}$	-17.01	7.34		7.34	1
$1f_{5/2}$	-18.01	8.34		8.34	1
$1f_{1/2}$	-19.01	9.34		9.34	1

Table 3.2 The proton spectrum. The proton single particle spectrum is obtained from the neutron single particle spectrum by moving the $g_{9/2}$ state to lie at λ.

Level	ε_a (MeV)	$\lvert(\varepsilon_a - \lambda)\rvert$ MeV
$1h_{11/2}$	-2.26	7.41
$2d_{3/2}$	-2.86	6.81
$3s_{1/2}$	-3.16	6.51
$1g_{7/2}$	-4.84	4.83
$2d_{5/2}$	-5.06	4.61
$1g_{9/2}$	-9.67	0
$2p_{1/2}$	-9.97	0.30
$2p_{3/2}$	-10.97	1.30
$1f_{5/2}$	-11.97	2.30
$1f_{7/2}$	-12.97	3.30

(b) The Self-Energy Insertions

As we pointed out in the introduction, our main premise is that the dressing of a single particle state in a nucleus occurs via two different processes : (1) the dressing $\Sigma_1^b(\omega)$ due to direct coupling to the compound states, and (ii) the dressing $\Sigma_1^d(\omega)$ due to the coupling to compound states via doorways. These two mechanisms are physically quite distinct. Let us discuss these in turn.

Table 3.2 The proton spectrum. The proton single particle spectrum is obtained from the neutron single particle spectrum by moving the $g_{9/2}$ state to lie at λ.

Level	ε_a (MeV)	$\lvert(\varepsilon_a - \lambda)\rvert$ MeV
$1h_{11/2}$	-2.26	7.41
$2d_{3/2}$	-2.86	6.81
$3s_{1/2}$	-3.16	6.51
$1g_{7/2}$	-4.84	4.83
$2d_{5/2}$	-5.06	4.61
$1g_{9/2}$	-9.67	0
$2p_{1/2}$	-9.97	0.30
$2p_{3/2}$	-10.97	1.30
$1f_{5/2}$	-11.97	2.30
$1f_{7/2}$	-12.97	3.30

(b) The Self-Energy Insertions

As we pointed out in the introduction, our main premise is that the dressing of a single particle state in a nucleus occurs via two different processes : (1) the dressing $\Sigma_1^b(\omega)$ due to direct coupling to the compound states, and (ii) the dressing $\Sigma_1^d(\omega)$ due to the coupling to compound states via doorways. These two mechanisms are physically quite distinct. Let us discuss these in turn.

(i) The background self-energy $\Sigma_1^b(\omega)$.

Since $\Sigma_1^b(\omega)$ is supposed to arise from the direct coupling of the many compound states surrounding it, its value is in principle calculable, but in practice impossible to determine. For even if the interactions were known, some form of selective summation of diagrams would be necessary, and this usually involves an adhoc approximation of some kind or another. However, we do know that the real part of $\Sigma_1^b(\omega)$ is essentially zero due to the random nature of contributions from the compound states lying above and below the energy ε_1, while the imaginary part is expected to be a slowly varying function of ω for the same reason. Consequently we can write

$$\Sigma_1^b(\omega) = \pm iW_1(\omega), \qquad W_1(\omega) \geq 0 \tag{3.8}$$

as in Eq (2.15), where we treat the matrix element $W_1(\omega) = \langle 1|W_{opt}(\omega)|1\rangle$ as a phenomenological function. Eq.(3.8) therefore identifies $W_{opt}(\omega)$ as the imaginary part of the nuclear optical potential. The phenomenology of this potential is well studied at positive energies, [Ui 64]. However we require $W_{opt}(\omega)$ (or rather its matrix elements) at negative energies for which much less is known. In this connection, one can appeal to Fermi liquid theory [Pi 66] , which predicts an $(\omega-\lambda)^2$ dependence near the Fermi surface, as well as the phenomenological fact that $W_1(\omega)$ is slowly increasing in the vicinity of zero energy, to make a plausible guess at the behavior of $W_1(\omega)$.

Two simple models suggest themselves :

(i) a quadratic model

$$W_1(\omega) = W_o\left(\frac{\omega-\lambda}{\lambda}\right)^2 \qquad (3.9)$$

or (ii) a linear model

$$W_1(\omega) = W_o\left|\frac{\omega-\lambda}{\lambda}\right| \qquad (3.10)$$

where W_o is the expected value of the optical potential at $\omega = 0$ (neutron threshold). As these expressions are meant to be extrapolations to negative values of ω in the vicinity of the Fermi energy, they should not be confused with the empirically known energy dependence of the optical potential for positive energies. When 1 refers to a hole state, we continue to use expressions (3.9) and (3.10). This involves yet a further assumption that the spreading of single particle states on either side of the Fermi surface is similar. While as yet there is no specific proof of this assertion, it does seem a reasonable one in view of the fact that a particle or hole state at the same distance from the Fermi surface will be confronted with a similar density of compound levels.

Such models of $W_1(\omega)$ as given by equations (3.9) and (3.10) are of course, gross approximations in a finite nucleus near $\omega=\lambda$, where in contrast to a Fermi liquid the very concept of an optical potential near the ground state looses all meaning. We will have to see how these assumptions work in practice. In view of all these uncertainties, it is clearly futile to pay attention to the state dependence of W ie to the label 1. So we accept equations (3.9) and (3.10) to hold irrespective of whether the state label refers to a particle or a hole. Thus our assumption for $W_1(\omega)$ is that it is symmetric about $\omega=\lambda$. The assumption of a specific form for $W_1(\omega)$ now allows one to calculate this function at the various excitation energies required for the calculation of the self-energy $\Sigma_1^d(\omega)$. We should perhaps emphasize that a more detailed analysis of the problem would introduce a phenomenological operator, W_{opt}, calculate its matrix elements, and try to deduce its parameters from a match between theory and experiment, as has been done for W_{opt} for positive energies in neutron scattering experiments. At the present time, however, there is not enough systematic data to make such an analysis a definitive one.

(ii.) The doorway self-energy $\Sigma_1^d(\omega)$

In contrast to $\Sigma_1^b(\omega)$, the self-energy $\Sigma_1^d(\omega)$ arises through the coupling of the single particle state 1 via doorway states to the compound states in its vicinity [Fs 67].

This feature assumes that the state 1 is only spread locally around the energy of the doorway state over an energy interval much smaller than the width $W_1(\varepsilon_1)$ of the single particle state. Consequently, we expect $\Sigma_1^d(\omega)$ to have both real (dispersive) and imaginary (absorptive) contributions, and to show structure as a function of ω in the vicinity of the doorway states it contains. Since we are considering the propagation of a single hole state in a nucleus, the generic structure of doorway states in our case consist of 2 hole - 1 particle excitations that lie in the vicinity of the single state. According to our model, the propagation of each particle or hole component in such a doorway state is described by the "better dressed" Green's function $G_1^b(\omega)$. Consequently each excitation of this type already has a spreading width associated with it that can be built up from the spreading widths of the individual components, as was illustrated by the construction of $\Sigma_1^d(\omega)$ from a single polarisation bubble, Eq.(2.45). We observe that the width of the excitation is given by

$$W_i(\omega-\varepsilon_j+\varepsilon_n) + W_j(\varepsilon_n+\omega-\varepsilon_i) + W_n(\varepsilon_j-\omega+\varepsilon_i) \qquad (3.11)$$

Since W is an increasing function of its arguments, this sum can easily become of the same order as the width of the original state 1, and the doorway state contribution would become indistinguishable from that of $\Sigma_1^b(\omega)$. This suggests that low-lying doorway states are the important ones in our problem. A second feature to bear in mind

is that our generic example of a doorway state is too naive. We know, for example, that residual interactions between the particle and hole forming the bubble can lead to a rescattering of these participants and thereby build up collective vibrations. Since the strength of the collective vibrations is built up at the expense of the non-collective particle-hole excitations, this redistribution of particle-hole strength becomes an important issue in the problem. One expects only the collective components of such particle-hole excitations to be visible as a significant energy variation in $\Sigma_1^d(\omega)$, since the non-collective states probably carry too little strength to show up as individual structures. These qualitative statements will be substantiated by further calculations.

(c) Structure of the Doorway States in ^{115}Sn.

We pointed out in the last section that doorway states having a collective character are expected to be particularly important in determining the energy dependence of $\Sigma_1^d(\omega)$. We now investigate possible doorways of this nature that could be relevant for dressing the $g_{9/2}$ antianalog quasihole state in ^{115}Sn. Two types of doorway states present themselves as candidates in this nucleus. These consist of a single neutron hole coupled to vibrations of the proton core (type I), or neutron valence shell (type II), respectively. If in the last case,

these doorway states have their neutron hole in the core, then, as explained in Sec.2.9b, such states do not by themselves conserve isospin. The correct linear combination for such type II doorway states is obtained [K] 2] by forming the analog state of a proton hole coupled to neutron valence shell vibrations in the parent system ^{115}In. It thus contains components more complex than 2 hole-1 particle excitations. A schematic representation of how both doorways appear in the shell model is given below:

TYPE I: 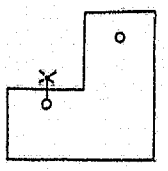

= ^{116}Sn core proton vibration plus neutron hole.

TYPE II: 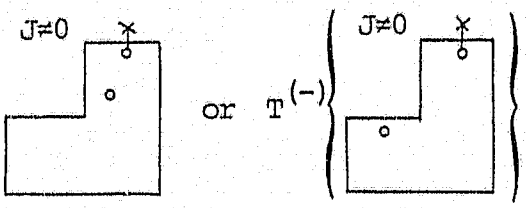

= analog of neutron vibration in ^{116}Sn core, plus proton hole.

Thus the type I doorway state represents a dressing of the $g_{9/2}$ quasihole by proton vibrations, while the type II dresses the $g_{9/2}$ quasihole with neutron vibrations. In the above picture, we have considered the proton core and neutron valence shell vibrations as occurring independently. This is not strictly true, however: the residual interaction will mix them. However, since the proton excitations are intershell, while the neutron vibrations intrashell, there is a relatively large energy separation (∿2-4 MeV) between their respective

these doorway states have their neutron hole in the core, then, as explained in Sec.2.9b, such states do not by themselves conserve isospin. The correct linear combination for such type II doorway states is obtained [K1 82] by forming the analog state of a proton hole coupled to neutron valence shell vibrations in the parent system ^{115}In. It thus contains components more complex than 2 hole-1 particle excitations. A schematic representation of how both doorways appear in the shell model is given below:

TYPE I: 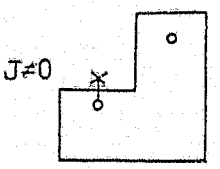

= ^{116}Sn core proton vibration plus neutron hole.

TYPE II: 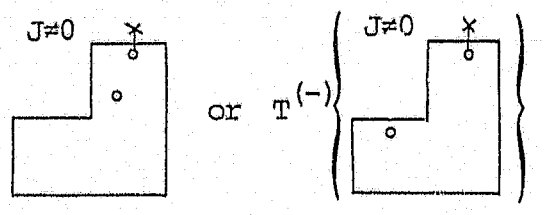

= analog of neutron vibration in ^{116}Sn core, plus proton hole.

Thus the type I doorway state represents a dressing of the $g_{9/2}$ quasihole by proton vibrations, while the type II dresses the $g_{9/2}$ quasihole with neutron vibrations. In the above picture, we have considered the proton core and neutron valence shell vibrations as occurring independently. This is not strictly true, however: the residual interaction will mix them. However, since the proton excitations are intershell, while the neutron vibrations intrashell, there is a relatively large energy separation (∿2-4 MeV) between their respective

excitation energies. Their mixing is consequently small. We continue to neglect it in what follows, and speak of these types of vibrations as though they occur as independent modes of excitation. A common feature of the spectra of the Tin isotopes is the occurrence of low-lying 2^+ and 3^- collective modes. In ^{116}Sn, these lie at $\hbar\omega_2$=1.27 MeV and $\hbar\omega_3$=2.38 MeV respectively [Be 69]. The expected positions of doorway states that can be formed by coupling these collective vibrations to those neutron hole states of Table 3.1 that can couple with them to a total angular momentum of $9/2^+$ are shown in Fig.3.5. The isobaric splitting [La 62] of the $g_{9/2}$ analog-antianalog pair is shown for comparative purposes. The estimated positions of type I doorways, based on a calculated value of $\hbar\omega_2$=3.8 MeV (see later) for a 2^+ collective mode of the proton core is shown by the broken lines. We have arbitrarily grouped those doorways involving the known 3^- excitation under type II: i.e. proton vibrations mainly. Whether this is predominantly so or not, is not relevant for our further discussion, since these doorway states lie too far from the $g_{9/2}$ quasihole to be significant.

It is clear from the level diagram in Fig.3.5 that the $g_{9/2}$ quasihole state remains relatively isolated except for the $[\tilde{g}_{9/2} \otimes 2^+]$ doorway just above it. The reasons for this are simply either the strong compression of the neutron quasiparticle spectrum or the large binding energies of the neutron quasiholes in the core. Both effects favor either low-lying or high-lying doorway states.

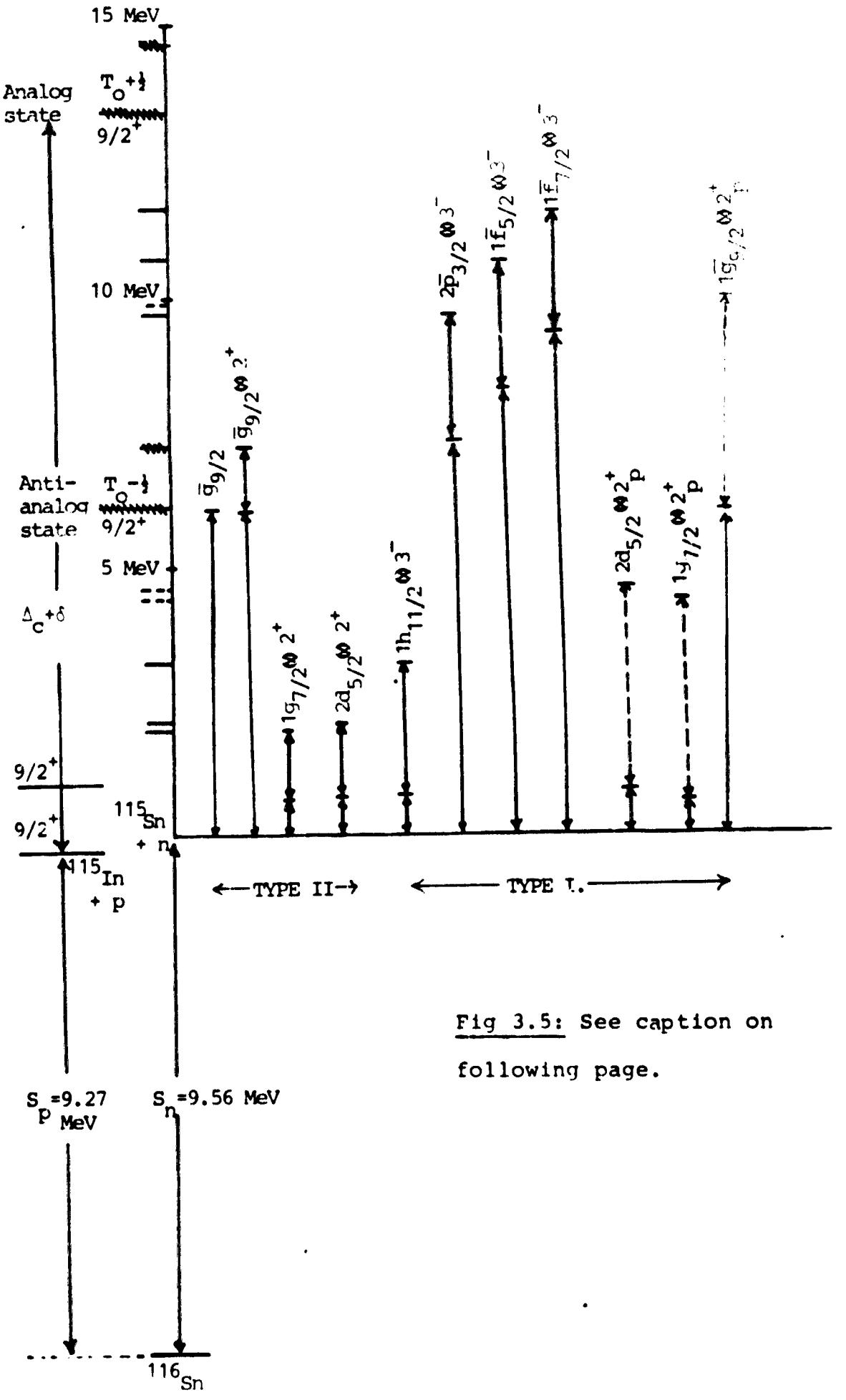

Fig 3.5: See caption on following page.

Fig.3.5: Energy-level diagram showing the relation of the one hole plus vibration doorway states to the $g_{9/2}$ analog and anti-analog states of ^{115}Sn. The experimental neutron and proton threshold energies for ^{116}Sn are also indicated. Δ_c and δ are the Coulomb energy shift and the neutron-proton energy difference respectively. The horizontal lines on the vertical axis mark the projections of the individual one hole plus vibration levels that have been individually identified by the excitations that make them up. The barred letters indicate neutron quasiholes, unbarred letters neutron (pairing) quasiparticles. The 2^+ and 3^- (experimental) collective modes at 1.27 and 2.38 MeV respectively, are shown on top of the single quasihole or quasiparticle they are combined with to form a doorway. The dotted lines give the same information for the calculated 2^+_p (proton core) vibration. The $g_{9/2}$ analog, anti-analog states and their accompanying doorways have been crosshatched for easy reference.

The latter lie at too low an excitation energy for the damping mechanism in our model to be physically realistic, while the former are effectively spread out to merge with the background because the model is certainly realistic in this region. To illustrate this effect, let us estimate the damping width of the component $2\bar{p}_{3/2} \otimes [2d_{5/2}\ 2\bar{p}_{1/2}]$ of the doorway state at 10 MeV excitation that contains the 3^- vibration. One has, from Eq.(3.11),

$$W_{2\bar{p}_{3/2}}(\varepsilon_{2\bar{p}_{3/2}})+W_{2d_{5/2}}(\varepsilon_{2d_{5/2}})+W_{2\bar{p}_{1/2}}(\varepsilon_{2\bar{p}_{1/2}}) \approx 1 \text{ MeV}$$

for the on-shell width, which is of the same order as the width of the $g_{9/2}$ quasihole (0.86 MeV).

Experimentally, [Ge 80], the $g_{9/2}$ quasihole strength function (see Fig.3.9 to follow later) shows significant fragmentation on its low energy side. We show in the following that these data are consistent with the presence of doorway states of the type II, consisting of a 2^+ collective mode due to vibrations of the proton core coupled to neutron holes. We estimate the position and strength of this collective mode from an RPA description of the proton core excitations, using the previously determined [Ki 60] P_2 part of the residual interaction that describes the neutron valence shell vibrations so successfully. This interaction may be written as $V(12)=-f_J\vec{Y}_J(1)\cdot\vec{Y}_J(2)$, where Y_{JM} is a spherical harmonic of rank J and f_J an adjustable (but for our case known) interaction strength. Its direct matrix elements cause the transfer of angular momentum J during particle-hole collisions. They are

$$(\overbrace{32|V|41}^{J}) = -f_J Q^J_{43} Q^J_{21} \qquad (3.12)$$

where

$$Q^J_{43} = (-)^{j_4+\frac{1}{2}}\left[\frac{(2j_4+1)(2j_3+1)}{4\pi}\right]^{\frac{1}{2}}(-)^{j_3+j_4+J}\begin{pmatrix} j_4 & j_3 & J \\ \frac{1}{2} & -\frac{1}{2} & 0\end{pmatrix}$$

$$\ell_4+\ell_3+J = \text{even}. \qquad (3.13)$$

It is well known [Br 72] that the eigenvalue equation, Eq.(2.62) for the RPA collective modes can be solved exactly if we approximate the direct matrix elements in that equation by Eq.(3.12), and suppress the exchange matrix elements. Then the RPA collective mode excitation energy becomes [Br 72]

$$\omega_c(\omega) = \mathcal{E}(\omega)\left[1 - \frac{2f_J}{\mathcal{E}(\omega)} \sum_{mi} (Q^J_{mi})^2\right]^{\frac{1}{2}} \tag{3.14}$$

with eigenvectors

$$x_{mi} = \frac{f_J Q^J_{mi}}{\mathcal{E}(\omega)-\omega_c(\omega)} \Lambda_c(\omega) \tag{3.15a}$$

$$\text{and} \qquad y_{mi} = \frac{f_J Q^J_{im}}{\mathcal{E}(\omega)+\omega_c(\omega)} \Lambda_c(\omega) \tag{3.15b}$$

The constant $\Lambda_c(\omega)$ is fixed by the normalisation condition Eq.(2.72) on the x's and y's to yield

$$|\Lambda_c(\omega)|^2 = \frac{(E^2+\Gamma(\omega)^2)}{\text{Re } \omega_c(E+i\Gamma(\omega))} \sum_{mi} (Q^J_{mi})^2 \tag{3.16}$$

The symbol

$$\mathcal{E}(\omega) = E - i\Gamma(\omega) \tag{3.17}$$

gives the average energy of the dressed particle-hole excitations that make up the vibrations ω_c. In particular, a 2^+ mode (which we henceforth designate 2^+_p) can be built up out of the proton excitations $1g_{9/2} \to 2d_{5/2}$ and $1g_{9/2} \to 1g_{7/2}$.

The high degeneracy of the $g_{9/2}$ state (containing 2j+1=10 protons) ensures the collective nature of the resulting vibration. To calculate its energy, we note by reference to Table 3.2 that the unperturbed energies of the above excitations are nearly degenerate: they lie at 4.6 and 4.8 MeV respectively. while their individual (on-shell) widths are $\Gamma=2.2(4.6/9.67)^2=0.50$ MeV and $\Gamma'=2.2(4.8/9.67)^2=0.54$ MeV respectively. This gives an average on-shell width of $\Gamma=0.52$ MeV. Hence

$$\mathcal{E} = (4.7 - 0.52i) \text{ MeV} \tag{3.19}$$

Actually, the imaginary part of $\mathcal{E}$ is energy dependent of course. Taking the quadratic form for $W_1(\omega)$ to construct $\Gamma(\omega)$, and setting $f_J=2.50$ MeV, a value bracketed by Kisslinger and Sorensen's value [Ki 60] of 2.75 MeV and the Bohr-Mottelson estimate[+] [Bo 75] of 2.04 MeV for the quadrupole-quadrupole strength, one finds the values of

$$\omega_c(\omega) = \alpha_c(\omega) - i\beta_c(\omega) \tag{3.20}$$

given in figures 3.6 and 3.7. One notes that the real part of the collective energy is lowered from 4.7 MeV to around 3.8 MeV by an amount almost independent of ω, while the imaginary part, $\beta_c(\omega)$, depends strongly on ω. The "on-shell" value is $\beta_c(\alpha_c)=0.67$ MeV.

[+] See Appendix D.

Fig. 3.6: Plot of $\alpha_c = \mathrm{Re}\omega_c(\omega)$ and $\beta_c = -\mathrm{Im}\omega_c(\omega)$ as a function of ω.

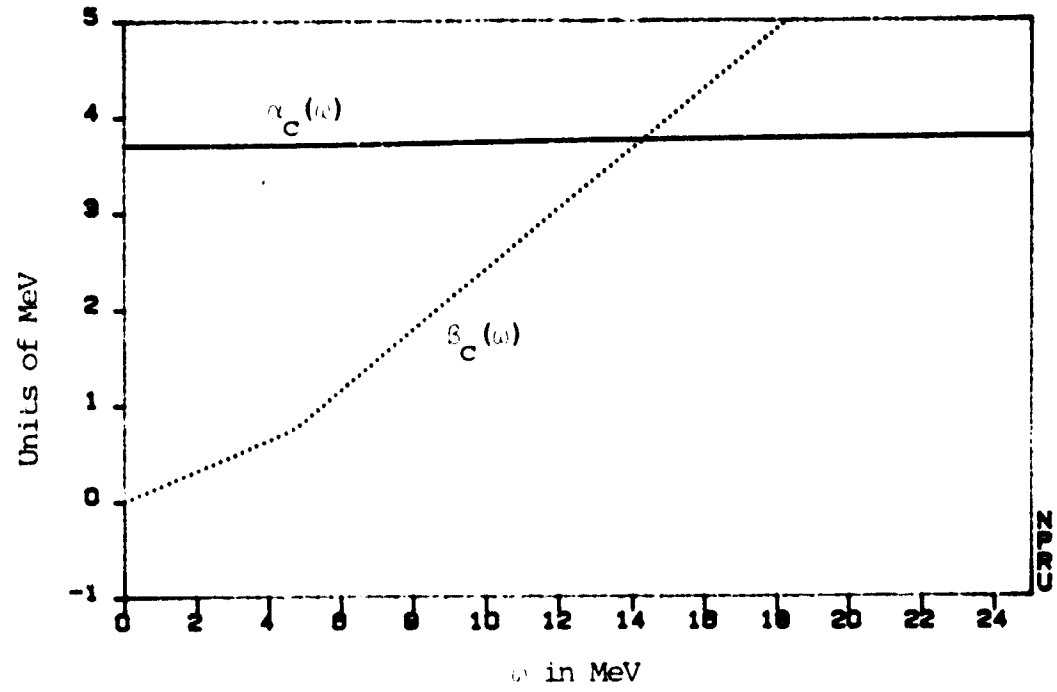

Fig. 3.7: Plot of $\beta_c(\omega)$ vs. $\alpha_c(\omega)$. Specific values of ω in steps of 2 MeV are indicated by the encircled points.

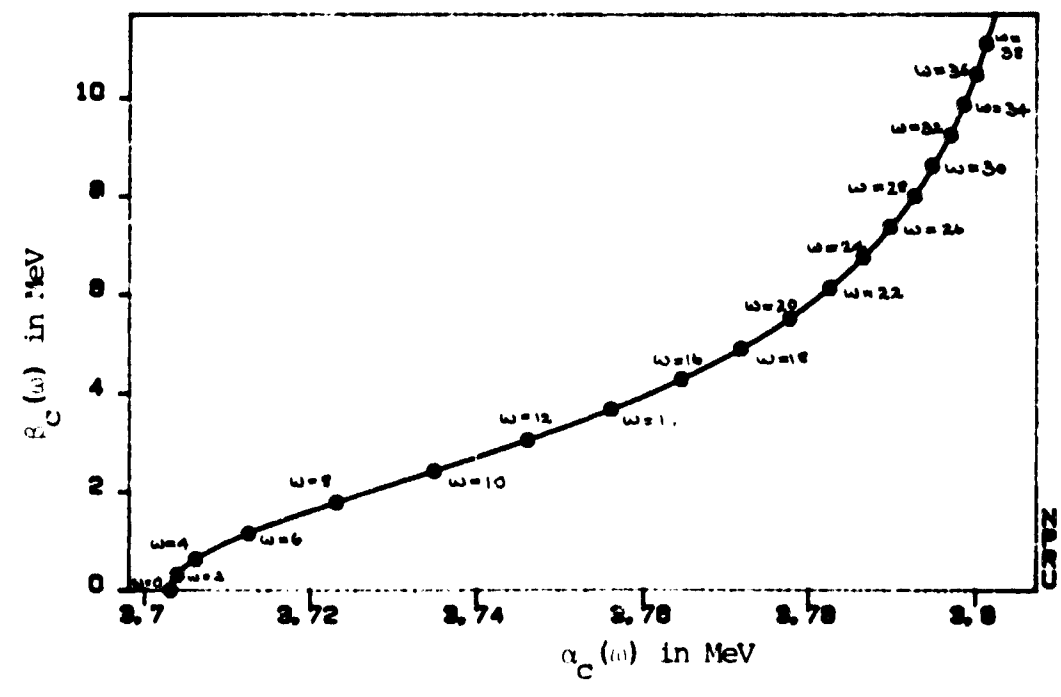

It now remains to couple the 2^+_p state to intermediate neutron hole (or quasiparticle) states as with the previous 2^+ and 3^- collective modes. Using $Re\omega_c \approx 3.8$ MeV, we obtain the set of dashed energy levels shown in Fig. 3.5. The requisite neutron parameters for computing $\Sigma^d_1(\omega)$ for the $g_{9/2}$ quasihole are given in Table 3.3.

Table 3.3: Data pertaining to the intermediate neutron state "2" required for the calculation of the self-energy $\Sigma^d_1(\omega)$ for the inclusion of the type I doorway state. Label 1 refers to the $g_{9/2}$ antianalog quasihole.

state (j_2)	$1g_{9/2}$	$2d_{5/2}$	$1g_{7/2}$
v^2	1.0	0.92	0.90
isospin factor $\frac{2T_o}{2T_o+1}$	YES	NO	NO
quasiparticle energy $\tilde{E}_a$ (MeV)	6.04	0.78	0.60

It is important to note that we will use the same interaction, viz. $-f_J \hat{Y}_J(1) \cdot \hat{Y}_J(2)$ for coupling the RPA dressed bubble $F_J(\underset{\rightarrow}{4}\underset{\leftarrow}{3}21,\omega)$ to the intermediate neutron state as was used to generate the bubble. In this regard, one can also see the collective enhancement of the coupling matrix elements by calculating $A^J_{12,\lambda}$ and $B^J_{12,\lambda}$ that are required in expression (3.7) for the separable interactions:

$$A^J_{12,\lambda} \equiv A^J_{12} = B^J_{12} = f_J^2 \, (Q^J_{12})^2 \, |\Lambda_c(\omega)|^2 \qquad (3.21)$$

where $|\Lambda_c(\omega)|^2 \sim \Sigma_{mi} \, (Q^J_{mi})^2$ shows the collective enhancement. Having calculated $\Sigma^d_1(\omega)$ in this fashion, we add it to $\Sigma^b_1(\omega)$ in accordance with Eq.(2.16) and hence construct $G_1(\omega)$ of Eq.(2.10'). The strength function is then given by

$$S_1(\omega) = \frac{1}{\pi} \, \mathrm{Im} G_1(\omega) \qquad (3.22)$$

This result refers to the isospin channel $T_o - \frac{1}{2}$. The neutron component of this, $S_1(\omega) \times 2T_o/(2T_o+1)$ is what is to be compared with experimental data. This comparison is discussed in the next section.

(d) Results.

In this section we show the results of calculating the $g_{9/2}$ neutron hole strength from Eq.(3.22) and make a comparison with experiment where possible. Figures 3.8 and 3.9 show this strength function for the isotope ^{115}Sn. The parameters entering the calculation have been described in detail in Sec.3.3(c). Both figures use the quadratic model for $W_1(\omega)$ for constructing the dressed Green's function $G^b_1(\omega)$ that enters into the calculation in an essential way as we have seen. Two choices for the strength W_o are illustrated. In Fig.3.8

this parameter is W_o=2.8 MeV, leading to a single particle absorptive potential of $W_1(0)$=1 MeV at threshold; Fig.3.10 uses exactly the same set of parameters as Fig.3.9, except for W_o=2.2 MeV, giving $W_1(0)$=0.8 MeV. In these, and in all subsequent figures, the experimental data of Gerlic et al. [Ge 80] has been shown as (i) a dashed histogram of the original data averaged over 0.5 MeV bins, and (ii), when there is sufficient data, as a dotted curve representing the measured strengths smoothed with a running Breit-Wigner weight function of width 0.3 MeV.

Fig 3.8: Calculated strength function for the $1g_{9/2}$ antianalog neutron quasihole in ^{115}Sn, plotted as a function of the binding energy (solid curve). The quadratic model has been used such that $W_1(0)$=1 MeV at threshold. Experimental data of Gerlic et al.[Ge 80] is indicated as a histogram and dotted curve as described in the text.

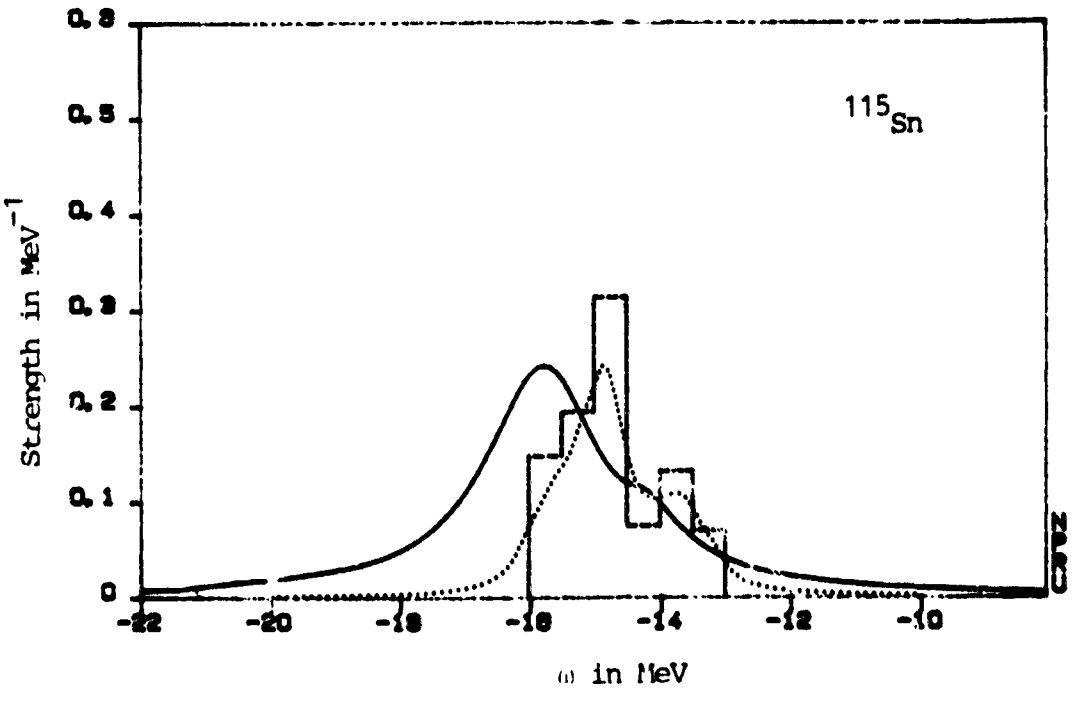

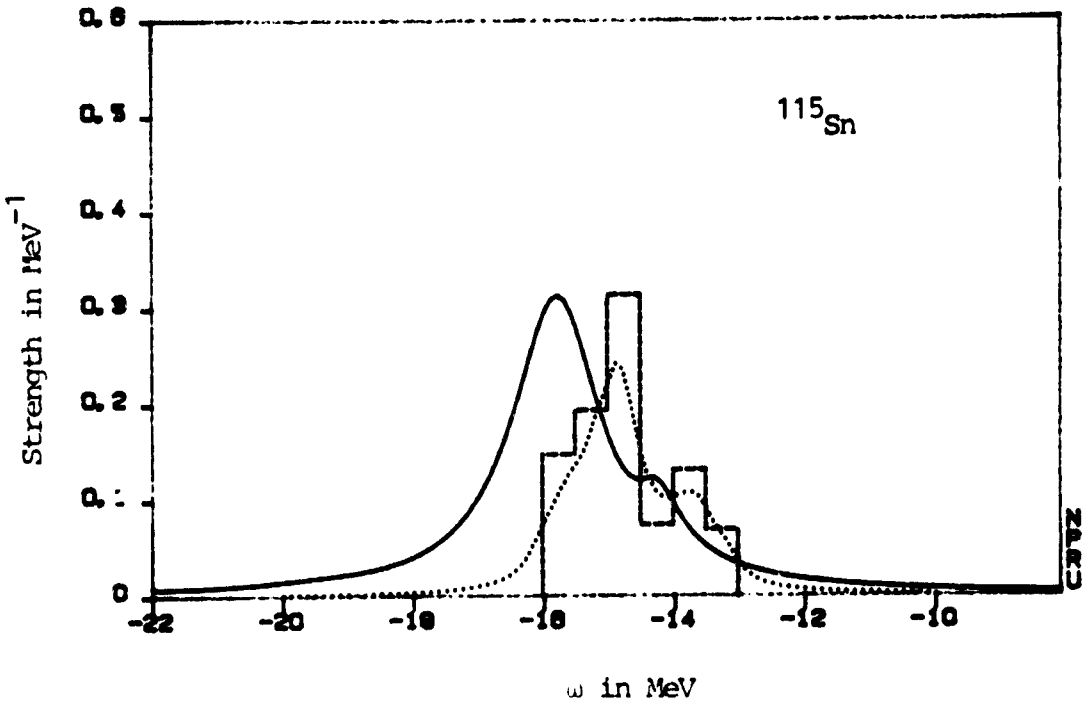

Fig. 3.9: $1g_{9/2}$ strength function as in Fig.3.8, but with W_o = 2.2 MeV.

The main peak observed in these two figures is the strength of the $1g_{9/2}$ antianalog state, while the shoulder immediately to the right of this, is due to the two overlapping doorway configurations, $2d_{5/2} \otimes 2^+_p$ and $1g_{7/2} \otimes 2^+_p$, see Fig. 3.5. The two peaks have been shifted slightly due to their mutual interactions. Note that this is a particular advantage of the Green's function formalism - one can go to the strength function directly, without prediagonalising in the space of one hole plus 2 hole-1 particle states. This has been automatically included in the calculation by the presence of $\Sigma^d_1(\omega)$ in $G_1(\omega)$.

Although the differences between figures 3.8 and 3.9 are qualitative rather than quantitative, the quadratic model for the energy variation of $W_1(\omega)$ appears to provide a better description of the features of the type I doorway state, than the linear model. This can be seen from Fig. 3.10 which shows the same calculation as presented in Fig. 3.9, except that it uses the linear model to ensure that $W_1(0)=0.8$ MeV at threshold. This requires $W_o=1.3$ MeV. The doorway state structure is much more smeared out in the linear model for $W_1(\omega)$ (which rises much too rapidly near the Fermi surface). By contrast, the expected width of this structure, ~400 keV, [K1 82] is well reproduced by the quadratic model.

Fig. 3.10: $1g_{9/2}$ quasihole strength function, using the linear form for $W_1(\omega)$, with $W_o=1.3$. This shows the same calculation as presented in Fig.3.9, except that the form of W is linear, not quadratic.

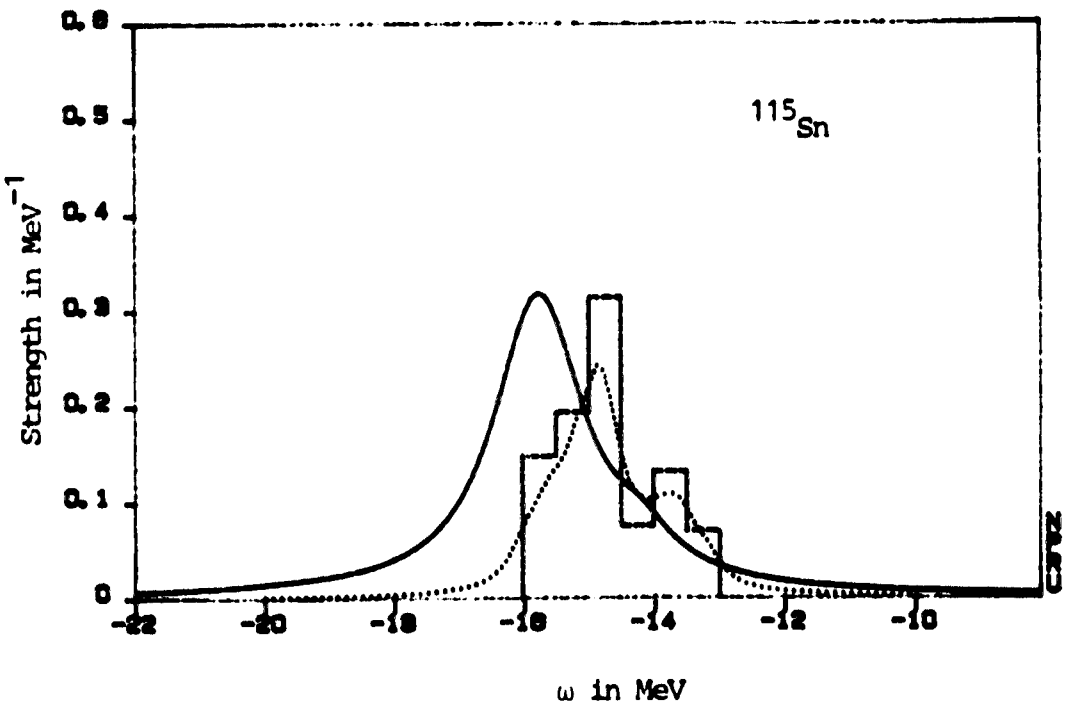

As can be seen in the preceding figures, the main peak of the calculated strength is not properly positioned, using the $g_{9/2}$ single particle energy of Gerlic. These energy values are of course, parameters in the shell model and one can readjust the calculated peak to lie at the observed position by raising all neutron single particle energies by 0.9 MeV. This is shown in figures 3.11 and 3.12:

Fig 3.11: $^{1}g_{9/2}$ antianalog quasihole strength function as depicted in Fig.3.8, but with all single particle energies raised by 0.9 MeV.

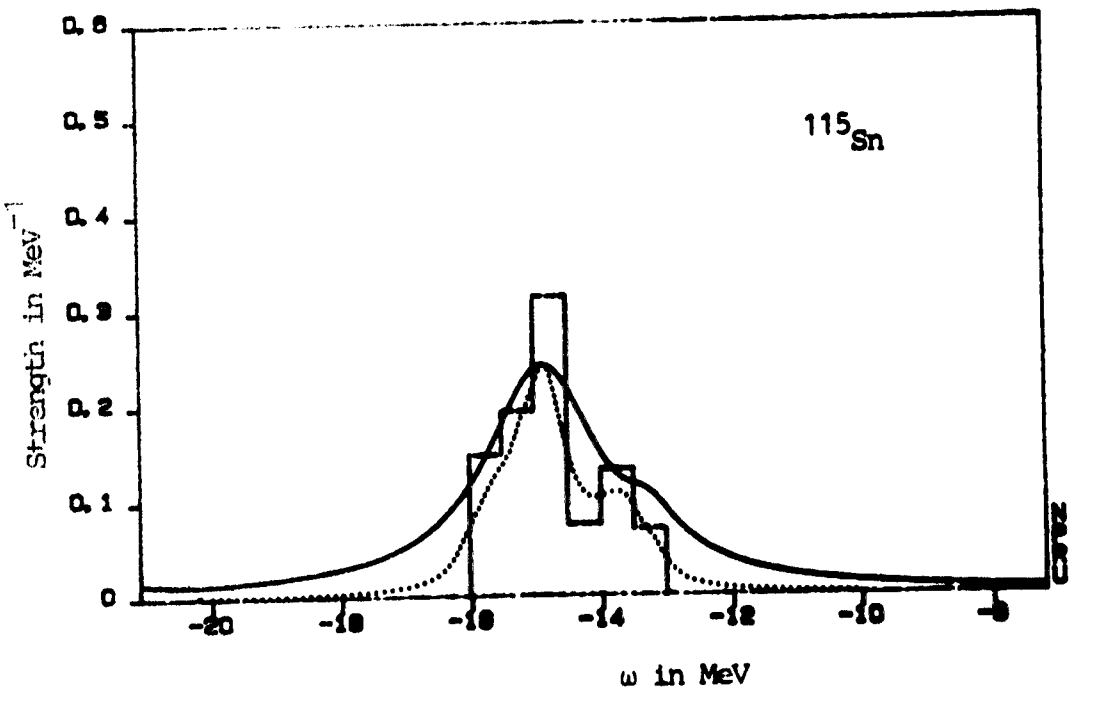

Fig.3.12: $1g_{9/2}$ antianalog quasihole strength function as depicted in Fig.3.9, but with single particle energies raised by 0.9 MeV.

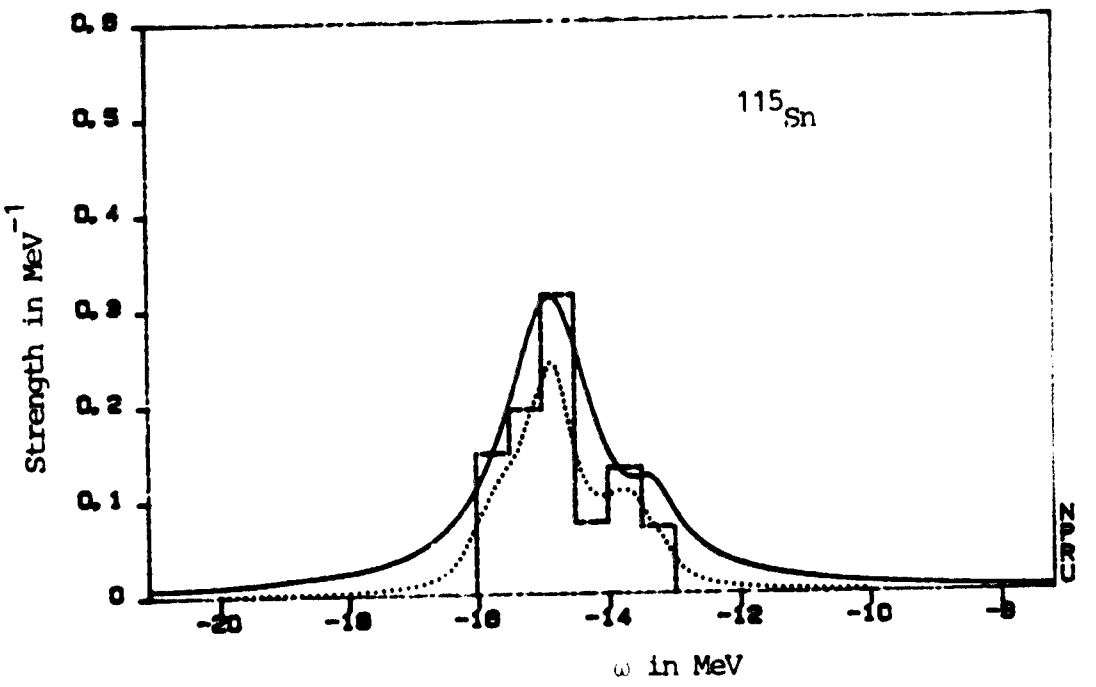

It is clear from the last two figures that an excellent description of the observed strength function is obtained from the model we have proposed. Not only is the splitting of the $g_{9/2}$ hole correctly reproduced by the coupling strength f_J that has been determined independently from other data, but also the width of both the main peak and its doorway satellite is correctly described. We take this latter feature as confirmation of the simple physical idea of building up the collective mode from quasiparticle states described by the "better dressed" Green's function, $G_1^b(\omega)$. It is a matter of opinion which of the above

calculations, which differ only in the value of the parameter W_o, give a better representation of the data.

It is also of interest to see what the model just described predicts for the $g_{9/2}$ strength function for the other isotopes of Sn. Referring back to Eq.(3.7) for the doorway self-energy $\Sigma_1^d(\omega)$, we realise that the only quantities entering this equation that are strongly dependent on mass number are the quasiparticle excitation energies E_a, and the occupation probabilities u_a^2 and v_a^2. The published calculations of Kisslinger and Sorensen allow one to follow the variation of these parameters through the Sn isotopes. Using these and resetting the Fermi level with respect to the neutron threshold from the neutron separation energy for each isotope, one obtains the sets of curves shown in figures 3.13 to 3.22.

Fig.3.13: Calculated $1g_{9/2}$ strength function for ^{109}Sn as in Fig. 3.12, but with parameters λ=0.29 MeV, Δ=0.98 MeV, and neutron separation energy of 11.18 MeV in ^{110}Sn.

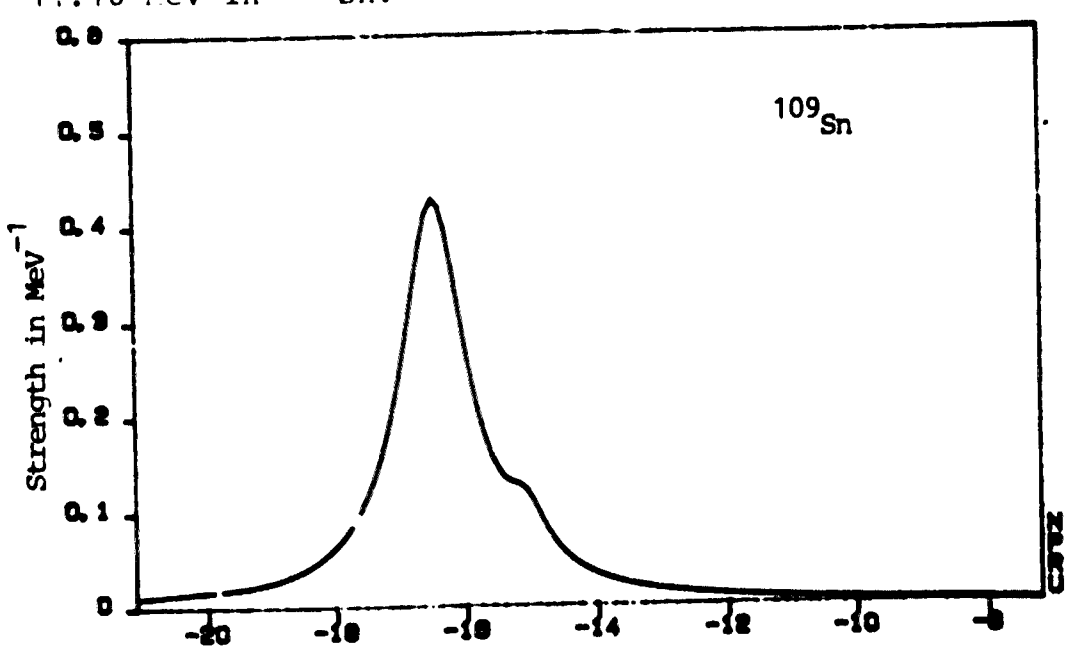

Fig. 3.14: Calculated $1g_{9/2}$ strength function for ^{111}Sn as in Fig. 3.12, but with parameters λ=0.60 MeV, Δ=0.97 MeV, and neutron separation energy of 10.79 MeV for ^{112}Sn. The data have been displayed as described in the text.

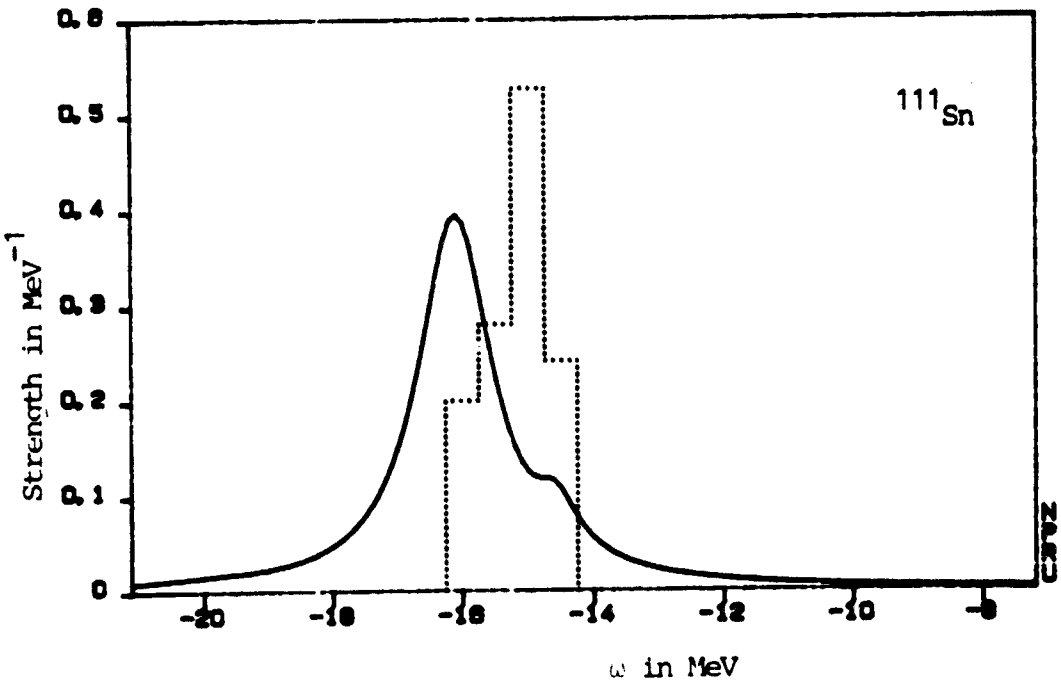

Fig. 3.15: Calculated $1g_{9/2}$ strength function for ^{113}Sn as in Fig. 3.12, but with parameters λ=0.97 MeV, Δ=0.90 MeV, and neutron separation energy of 10.29 MeV for ^{114}Sn.

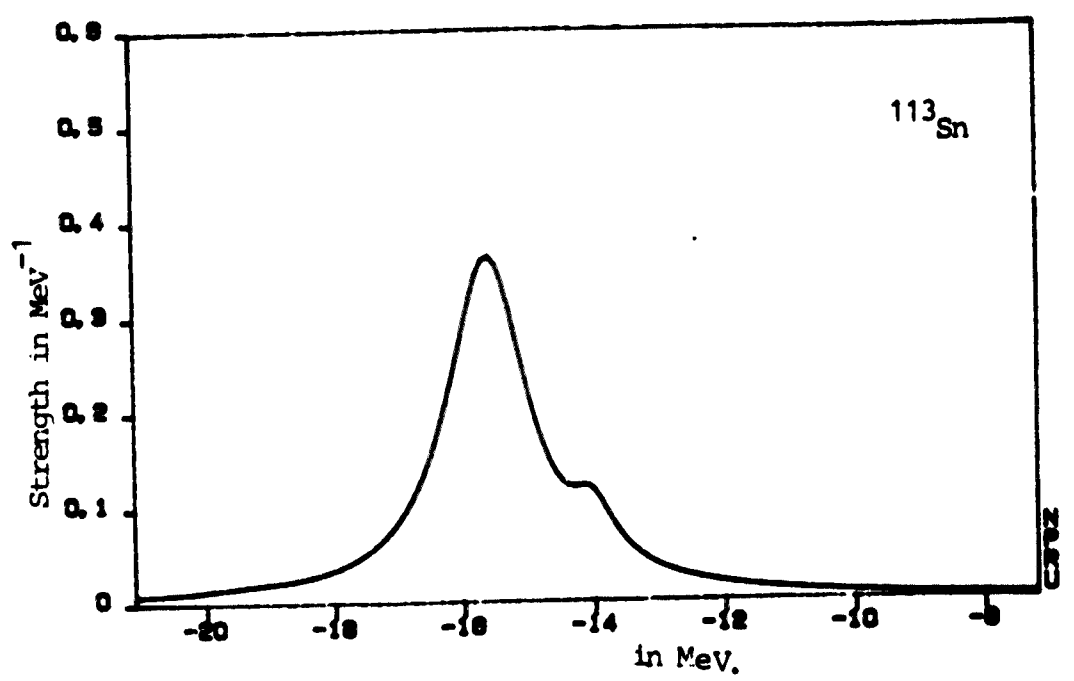

Fig. 3.16: Calculated $1g_{9/2}$ strength function for ^{117}Sn as in Fig. 3.12, but with parameters λ=1.81 MeV, Δ=1.00 MeV, and neutron separation energy in ^{118}Sn of 9.33 MeV.

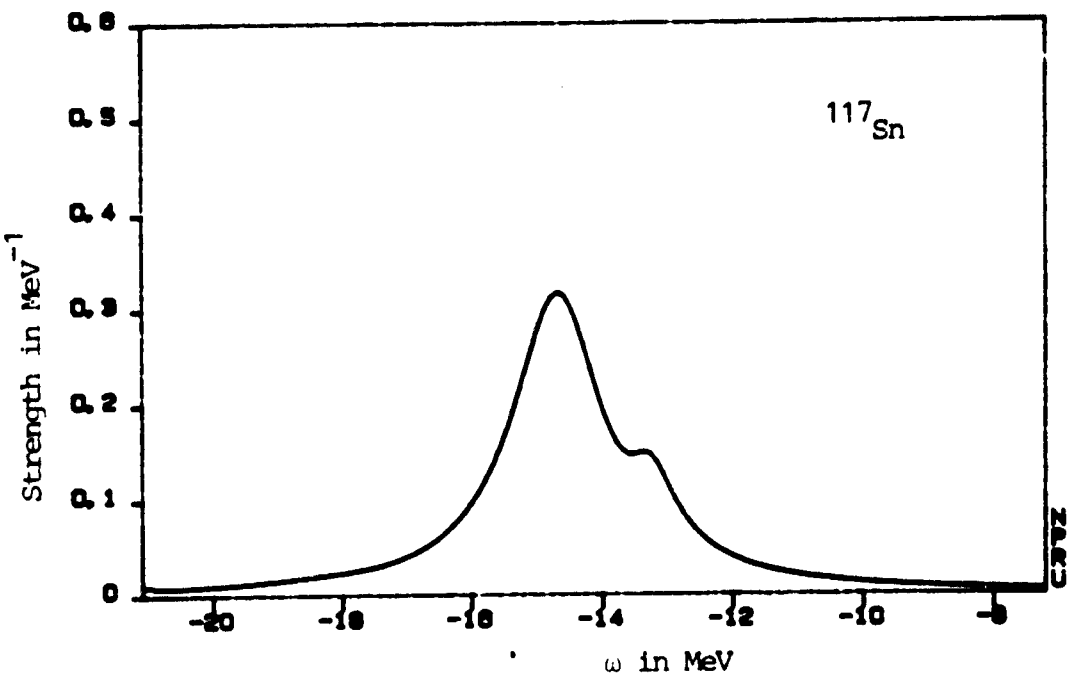

Fig. 3.17: Calculated $1g_{9/2}$ strength function for ^{119}Sn as in Fig. 3.12, but with parameters λ=2.12 MeV, Δ=1.05 MeV, and neutron separation energy of 9.10 MeV in ^{120}Sn. The data have been displayed as described in the text.

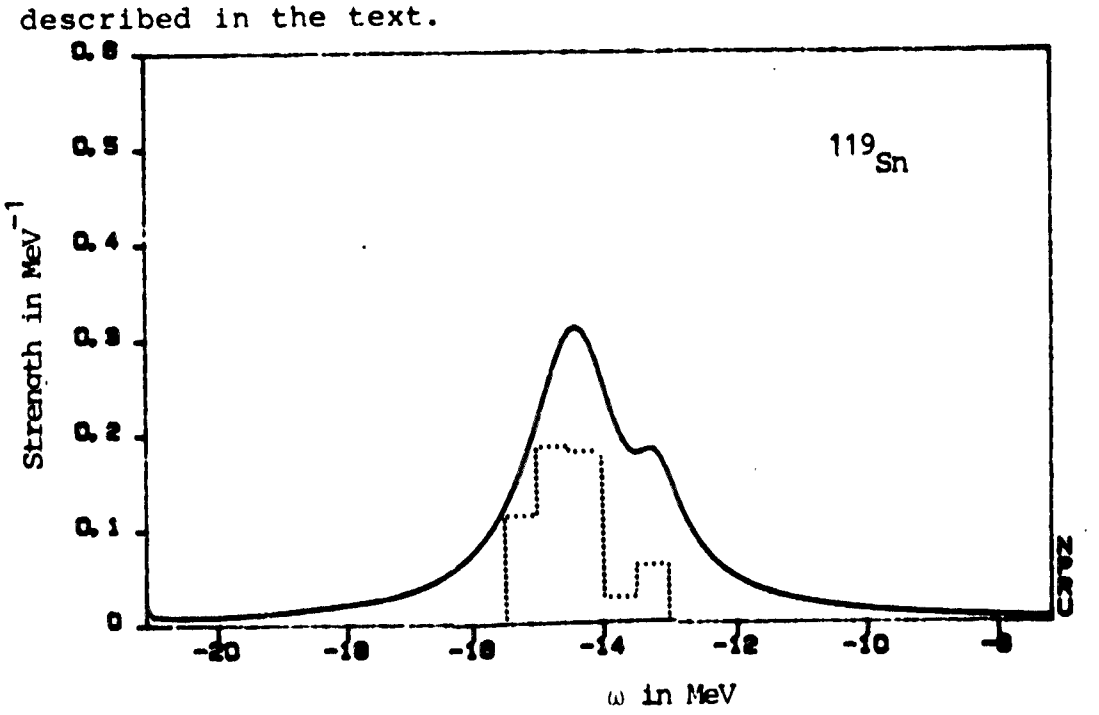

Fig. 3.18: Calculated $1g_{9/2}$ strength function for ^{121}Sn as in Fig. 3.12, but with parameters λ=2.40 MeV, Δ=1.08 MeV, and neutron separation energy of 8.81 MeV for ^{122}Sn.

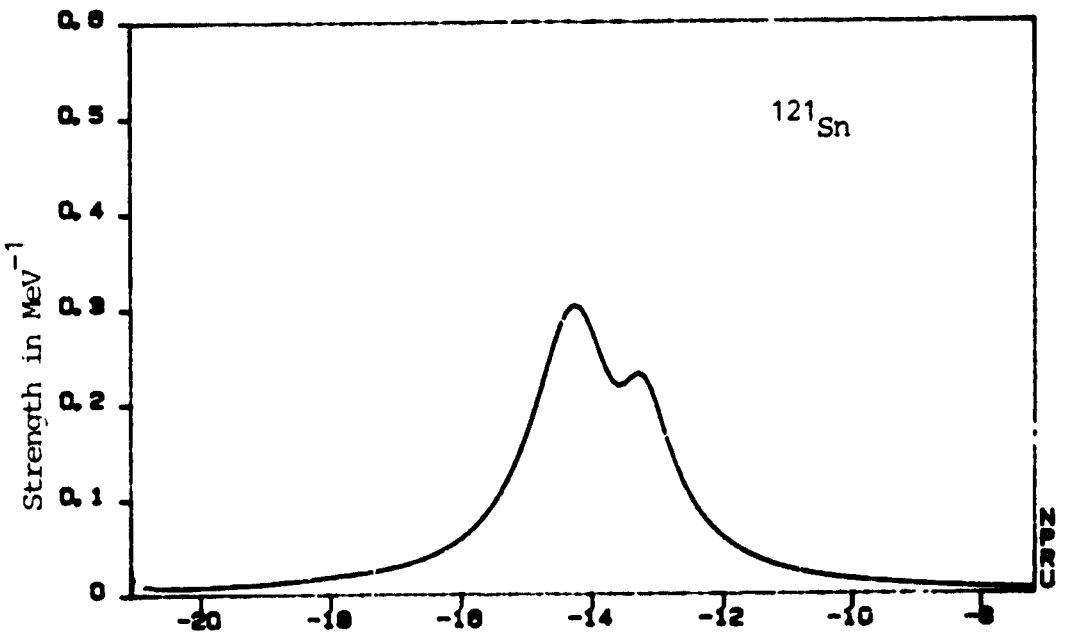

Fig. 3.19: Calculated $1g_{9/2}$ strength function for ^{123}Sn as in Fig. 3.12, but with parameters λ=2.65 MeV, Δ=1.06 MeV, and neutron separation energy of 8.49 MeV for ^{124}Sn.

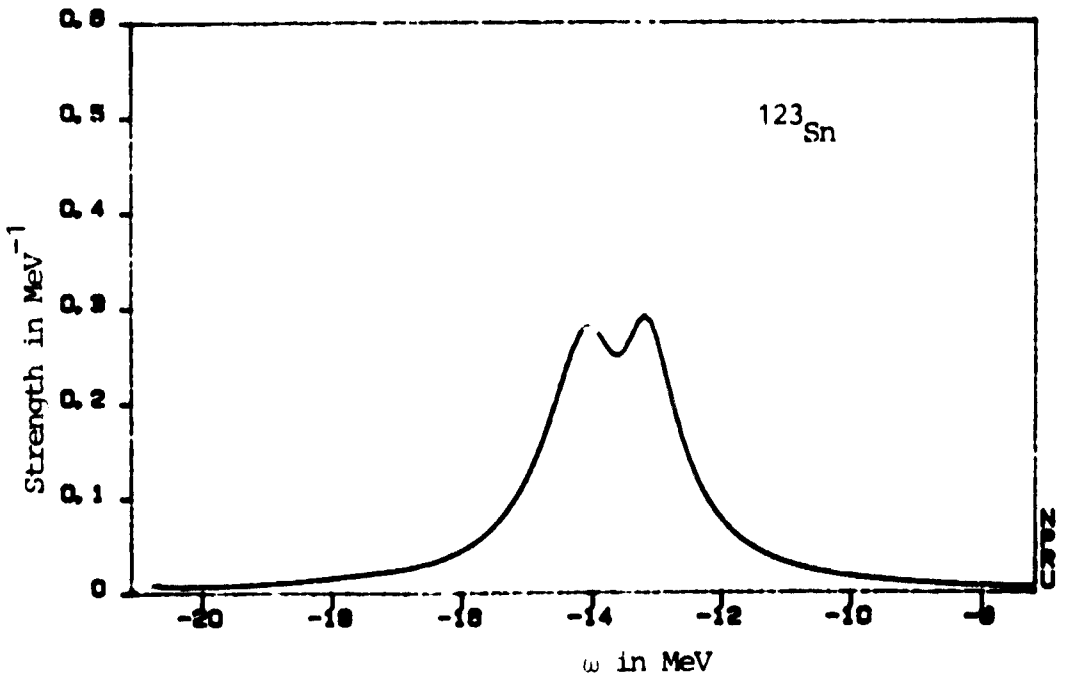

Fig. 3.20: Calculated $1g_{9/2}$ strength function for ^{125}Sn, as in Fig. 3.12, but with parameters λ=2.88 MeV, Δ=1.00 MeV, and neutron separation energy of 8.20 MeV for ^{126}Sn.

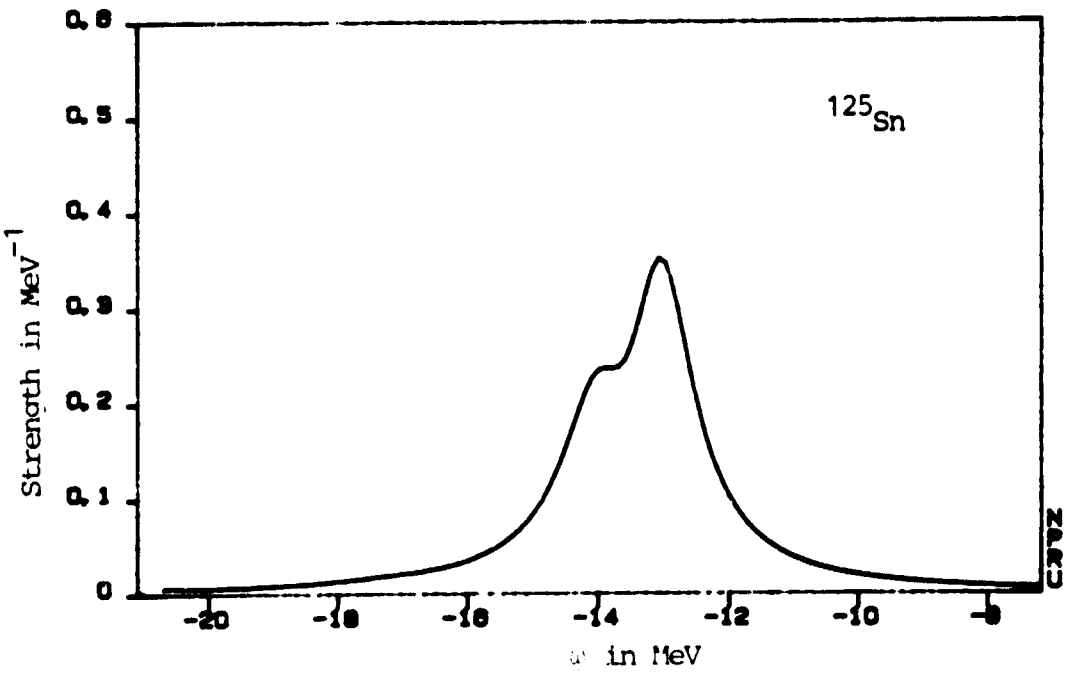

Fig. 3.21: Calculated $1g_{9/2}$ strength function for ^{127}Sn, as in Fig. 3.12, but with parameters λ=3.12 MeV, Δ=0.90 MeV and neutron separation energy of 7.96 MeV for ^{128}Sn.

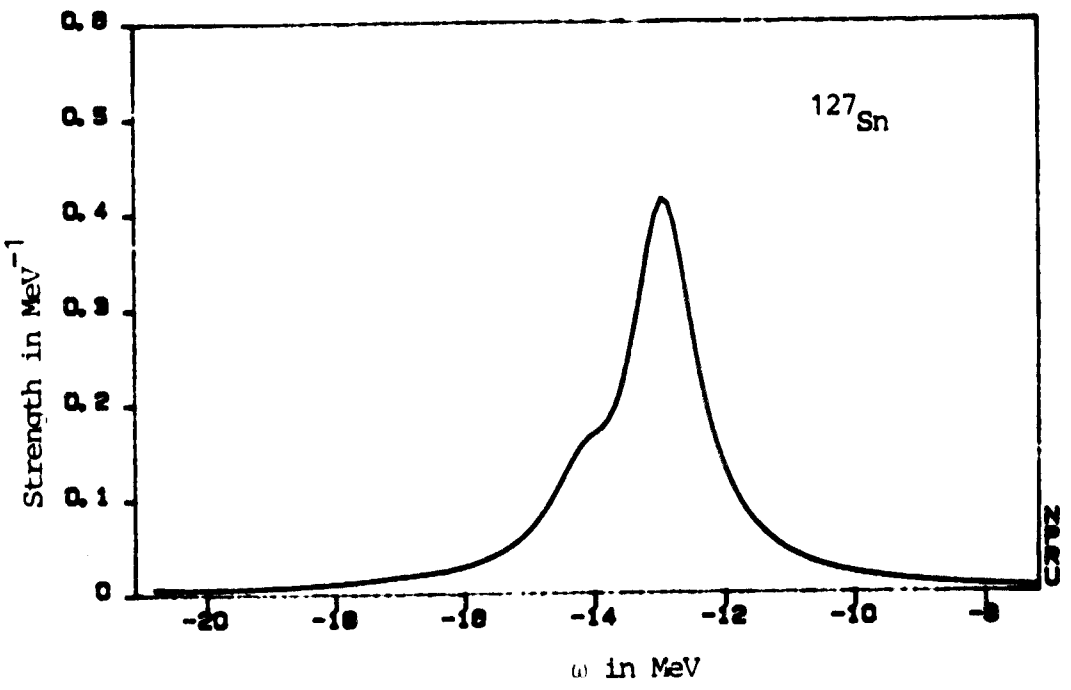

Fig. 3.22: Calculated $1g_{9/2}$ strength function for ^{129}Sn, as in Fig. 3.12, but with parameters λ=3.36 MeV, Δ=0.72 MeV, and estimated neutron separation energy of 7.80 MeV for ^{130}Sn.

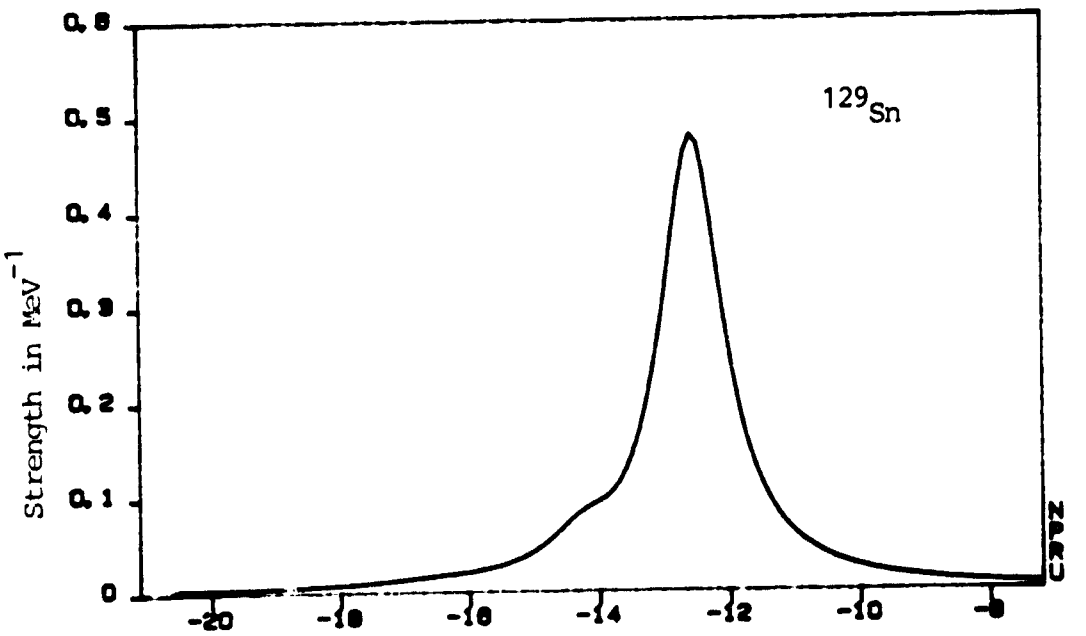

We have supplied the experimental data where available, in the form of a histogram, averaged over 0.5 MeV energy bins. Two features should be pointed out. Firstly, one notices that the doorway state shifts considerably in energy as one moves through the Sn isotopes. This is brought about by the strong mass number dependence of the quasiparticle energies E_a. Secondly, one sees that the fits predicted for $^{111,119}Sn$ are very satisfactory, without any further adjustment of the remaining parameters that were used for ^{115}Sn.

We conclude this section by pointing out that the other doorway states appearing in Fig. 3.5 have little effect

on the $g_{9/2}$ quasihole due to their energy separation or (on the high energy side) large damping. It is of interest to note however, that two of the three low-lying doorways formed by coupling the 3^- or 2^+ vibrations to the $2d_{5/2}$, $1g_{7/2}$ and $1h_{11/2}$ neutron quasiparticle have been identified with observed states $9/2^+$ at 2.37 and 3.07 MeV in the pick-up data of Gerlic et al., [Ge 80].

CHAPTER 4.

DISCUSSION AND OUTLOOK.

While the results of the model for calculating the strength function for deep-lying holes and their comparison with experiment are rather self evident, some concluding remarks are in order. We first examine the basic assumption, as embodied in Eq.(2.16), that the self-energy can be split into a smoothly-varying piece $\Sigma_1^b(\omega)$ and a doorway piece $\Sigma_1^d(\omega)$. The two extremes of this assumption are (i) there is no background contribution. All damping of the hole state proceeds via doorway states to which it is coupled locally. One can easily test this idea by shutting off $\Sigma_1^b(\omega)$ in $G_1(\omega)$ but not in $G_1^b(\omega)$. This has been done in Fig.4.1. The resulting peakheight of the $g_{9/2}$ state is seen to be much too high, the width much too narrow. (ii) There is no doorway contribution, $\Sigma_1^d(\omega)$ is zero. Then the $g_{9/2}$ strength function consists of a single, unsplit peak, [K1 82].

The question of how $\Sigma_1^b(\omega)$ behaves with energy is a second basic assumption that we have had to introduce. The device, proposed in Sec. 2.3 of relating $\mathrm{Im}\Sigma_1^b(\omega)$ to $W_1(\omega)$, the average value of the nuclear optical potential at energy ω is certainly a reasonable one, especially in

view of the excellent results that have been obtained from it. From a more fundamental point of view, the implementation of this assumption is more troublesome: experiment does not give us information on the "off-shell" values of $W_1(\omega)$ when $\omega \neq \varepsilon_1$. We got around this problem by arguing that details of how $W_1(\omega)$ depends on its state label "1" could not be identified from our calculations in view of the sparseness of the data. While this is certainly true, the question is a very interesting one that will certainly have to be answered as more data becomes available that <u>does</u> require a better knowledge of $W_1(\omega)$. The situation has a strong parallel with the development of the optical potential at positive energies.

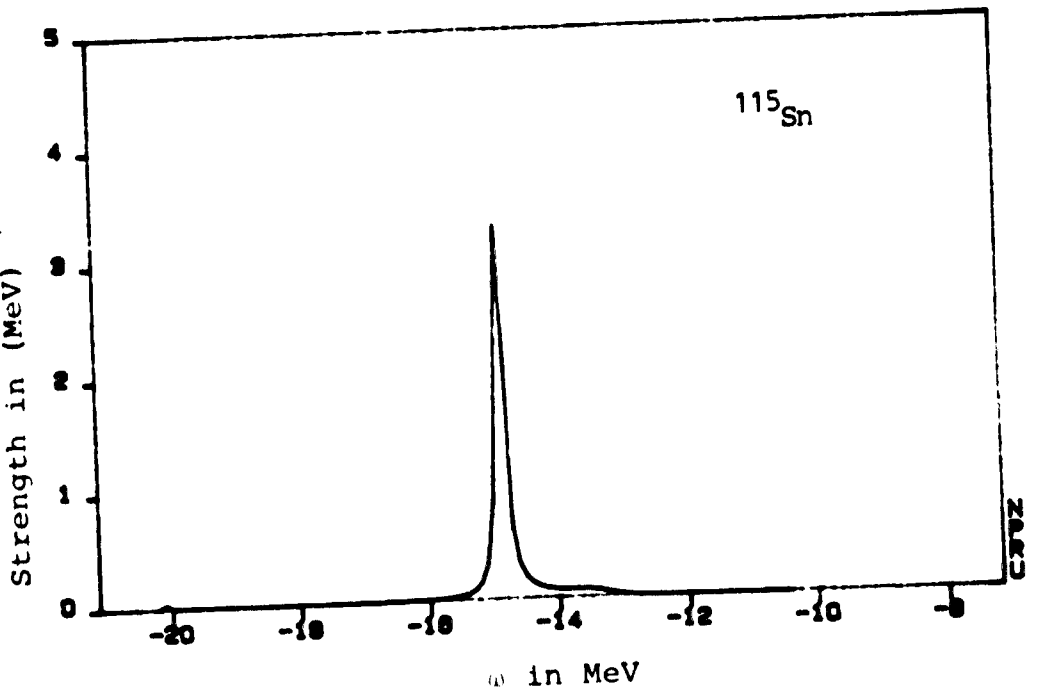

<u>Fig. 4.1:</u> Calculated $1g_{9/2}$ strength function for ^{115}Sn, using parameters as in Fig. 3.12, but suppressing the background self-energy $\Sigma_1^b(\omega)$.

After the initial phenomenological success, the availability of more and better data has resulted in rather detailed empirical knowledge of the properties of the nuclear absorptive potential. This empirical detail has also provided the necessary impetus to carry out a reasonably successful derivation of the nuclear optical potential from a more microscopic viewpoint [Vo 79]. In the case of hole states one can expect parallel developments as more data become available. For deep-lying holes, development of a microscopic theory would be of special interest, since the off-shell behavior of $W_1(\omega)$ enters into the determination of the doorway state spreading widths in an essential way.

The model assumptions we have introduced in discussing the strength function problem also have advantages. The reader will have noted that, while many of the ideas of the nuclear shell model have been used, none of its details enter the actual calculations. That this should be appropriate is perhaps not too suprising in retrospect. One knows, for example, from the many successes of the pairing model for open shell vibrations, or the pure RPA for the vibrations of closed shells, that the main ingredients of the physics are adequately modelled in terms of effective interactions between nucleons that occupy single particle states in some average field. The matrix elements determining the size of the effective interaction and the single particle energies of the average field are then treated as parameters. Only in a more detailed

(e.g. Hartree Fock) description would one attempt to calculate single particle energies, and from this, the wave functions that determine in turn, the matrix elements of the effective interaction.

In our case, the only really adjustable parameters are the single particle binding energies of the average field, although for the $g_{9/2}$ q in particular, this is fairly well determined via the known analog state location and its isobaric splitting due to the symmetry energy, see Fig. 3.5. As pointed out, the other parameters like the interaction strength f_J and the strength W_o of the absorptive potential are rather accurately determined from a variety of independent data. The fact that these parameter values lead to such excellent agreement with the data when used in conjunction with the assumptions of our theory, is a strong indication that we have succeeded in isolating the main physical features of the damping mechanisms for deep-lying holes.

APPENDIX A.

Guide to Feynman Diagrams.

The interpretation of diagrams tabulated below summarizes the conventions set out by R.D. Mattuck [Ma 76]; for detailed information on how the diagrams are related to the Interaction Picture expansion of the single particle Green's function, see Appendices E to G of this reference. Note that only those diagrams which are essential to calculations within this work are listed. Furthermore, unless otherwise stated, all diagrams are meant in the Feynman sense (i.e. the single particle Green's functions, and all expressions calculated from them, are time ordered.) On occasion it has been useful to illustrate the meaning of a diagram in the Goldstone sense. This means that a particular time ordering in the single particle Green's function is chosen, as given in table A2.

Table A1: "Diagram Dictionary" for an interacting fermion system, interpreted in the Feynman sense (i.e. all quantities are time ordered.).

Diagram	Factor associated	Meaning
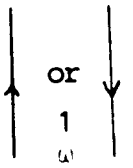	$iG_1^{(0)}(\omega)$	Non-interacting (HF) single particle Green's function.
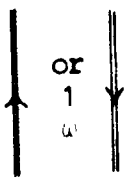	$iG_1^b(\omega)$	Single particle Green's function, dressed by background self-energy $\Sigma_1^b(\omega)$.
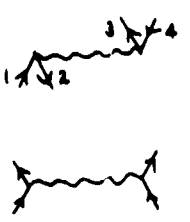	$-i(32\|\tilde{V}\|41)$	direct minus exchange matrix element of the two-body interaction potential
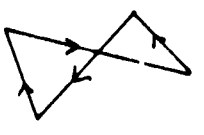	(-) for each closed loop.	
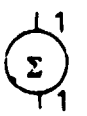	$-i\Sigma_1(\omega)$	self-energy
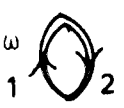	$-i\Pi(12,\omega)$	Single dressed polarisation bubble.

/cont...

Table A1 cont:

Diagram	Factor associated	Meaning
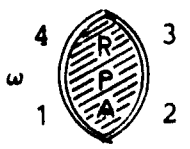	$-iF(4321,\omega)$	Particle-hole propagator in the Random Phase Approximation. (see Sec. 2.3)
	$\int \frac{d\omega}{2\pi}$ for each intermediate frequency.	

Where it has been useful to view diagrams in the Goldsto sense, no translation of diagrams has been necessary. For completeness, however, the associated symbols are included in Table A2.

/cont...

Table A2: "Diagram Dictionary" for an interacting fermion system, interpreted in the Goldstone sense. (i.e. time ordering specified).

Diagram	Factor associated	Meaning
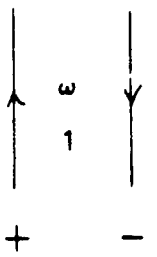	$iG_1^{\pm}(\omega)$	Retarded (+) or advanced (−) non-interacting single particle Green's functions.
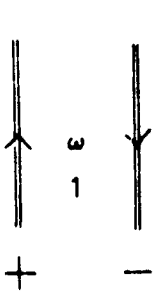	$iG_1^{b\pm}(\omega)$	Retarded (+) or advanced single particle Green's functions, dressed with $\Sigma^b(\omega)$.
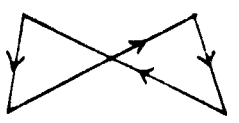	(−) for each fermion loop.	
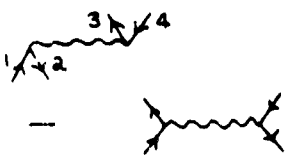	$-i(32\|V\|41)$	Matrix element of two body interaction.
	$\int \frac{d\omega}{2\pi}$ for each intermediate frequency.	

Note that the relationship connecting the time-ordered, retarded, and advanced propagators, is simply:

$$G_1(t) = G_1^+(t) \qquad t>0$$

$$= G_1^-(t) \qquad t<0$$

APPENDIX B.

Calculation of $\P(hp,\omega)$

The purpose of this appendix is to explain the rationale of a technique used often during the course of this thesis to evaluate sums of the form

$$\P(hp,\omega) = \sum_{ss'} \frac{|(c_h)_{s'o}|^2 |(c_p^+)_{so}|^2}{\omega+\varepsilon_s+\varepsilon_{s'}-i\eta} \qquad (B1)$$

The problem in evaluating a sum of this nature is that the function W_h, which occurs in $|(c_h)_{s'o}|^2$, depends on ε_s, in an unknown manner, and the function W_p, which occurs in $|(c_p^+)_{so}|^2$ depends on ε_s in an unknown manner too. It is therefore necessary to deal with the dependence of W_h and W_p on ε_s and $\varepsilon_{s'}$ in an approximate way, in order to do the summation. We therefore look for and isolate important values of ε_s and $\varepsilon_{s'}$ in the summand. To do this, consider

$|(c_p^+)_{so}|^2$ depends on ε_s in an unknown manner too

$$\text{Im}\ \P(hp,\omega) = \sum_{ss'} |(c_p^+)_{so}|^2 |(c_h)_{s'o}|^2 \frac{\eta}{(\varepsilon_s+\varepsilon_{s'}+\omega)^2+\eta^2} \qquad (B2)$$

If $|(c_p^+)_{so}|^2$ and $|(c_h)_{s'o}|^2$ are slowly varying, then the major contribution will come from $\omega=-\varepsilon_s-\varepsilon_{s'}$, and we may decouple the sum as follows:

APPENDIX B.

Calculation of $\P(hp,\omega)$

The purpose of this appendix is to explain the rationale of a technique used often during the course of this thesis to evaluate sums of the form

$$\P(hp,\omega) = \sum_{ss'} \frac{|(c_h)_{s',o}|^2 |(c_p^+)_{so}|^2}{\omega+\varepsilon_s+\varepsilon_{s'},-i\eta} \qquad (B1)$$

The problem in evaluating a sum of this nature is that the function W_h, which occurs in $|(c_h)_{s',o}|^2$, depends on $\varepsilon_{s'}$ in an unknown manner, and the function W_p, which occurs in $|(c_p^+)_{so}|^2$ depends on ε_s in an unknown manner too. It is therefore necessary to deal with the dependence of W_h and W_p on ε_s and $\varepsilon_{s'}$ in an approximate way, in order to do the summation. We therefore look for and isolate important values of ε_s and $\varepsilon_{s'}$ in the summand. To do this, consider

$$\text{Im}\ \P(hp,\omega) = \sum_{ss'} |(c_p^+)_{so}|^2 |(c_h)_{s',o}|^2 \frac{\eta}{(\varepsilon_s+\varepsilon_{s'}+\omega)^2+\eta^2} \qquad (B2)$$

If $|(c_p^+)_{so}|^2$ and $|(c_h)_{s',o}|^2$ are slowly varying, then the major contribution will come from $\omega=-\varepsilon_s-\varepsilon_{s'}$, and we may decouple the sum as follows:

$$\mathrm{Im}\P(hp,\omega) = \sum_{ss'} |(c_p^+)_{so}|^2 |(c_h)_{s'o}|^2 \varepsilon_{s'=-\varepsilon_s-\omega}$$

$$\times \sum_{s} \frac{\eta}{(\varepsilon_s+\varepsilon_{s'}+\omega)^2+\eta^2}$$

$$\approx \frac{\pi}{D_{s'}} \sum_{s} |(c_h)_{s'o}|^2 |(c_p^+)_{so}|_{\varepsilon_{s'=-\varepsilon_s-\omega}} \qquad \text{(B3)}$$

$\overline{|(c_p^+)_{so}|^2}$ and $\overline{|(c_h)_{s'o}|^2}$ peak at $\varepsilon_s=\varepsilon_p-\lambda$ and $\varepsilon_{s'}=\lambda-\varepsilon_h$ respectively (see Eq.(2.29)). These may be given on the same scale by employing the restriction $\omega=-\varepsilon_s-\varepsilon_{s'}$. Then $\overline{|(c_p^+)_{so}|^2}$ peaks at $\varepsilon_{s'}=-(\varepsilon_p-\lambda)-\omega$. This is represented schematically in Fig.B1.

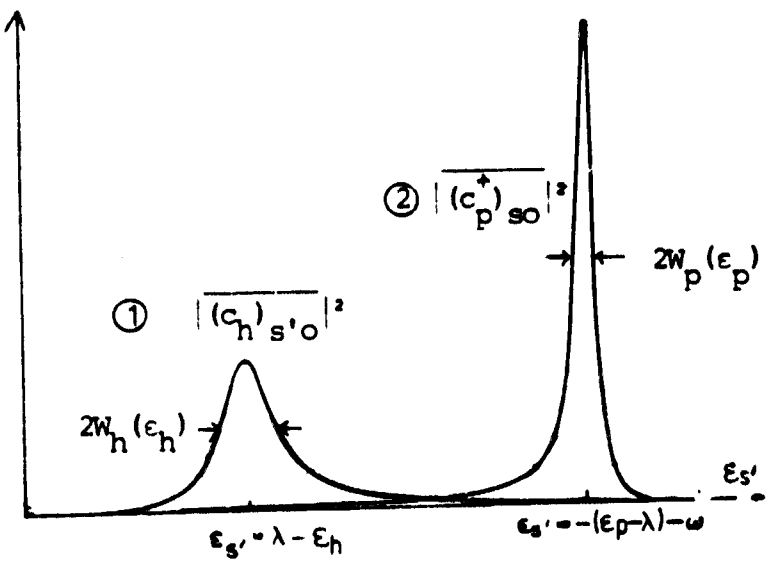

Fig. B1: Schematic representation of the strength functions $\overline{|(c_h)_{so}|^2}$ and $\overline{|(c_p^+)_{so}|^2}$ subject to the condition $\omega=-\varepsilon_s-\varepsilon_{s'}$, as is necessary for the calculation of $\mathrm{Im}\P(hp,\omega)$.

We assume that the curves are sharply peaked, and are separated by a distance such that only their tails

overlap. Suppose the tail of one resonance is taken as approximately constant over the resonance region of the other, and vice-versa. Then Eq. (B3) represents the area under the product of these two functions, which we may approximate as:

$$\text{Area} \approx (\text{area under curve (1)}) \times (\text{value of (2) at resonance (1)}) + (\text{area under curve (2)}) \times (\text{value of (1) at resonance (2)}) \tag{B4}$$

i.e.

$$\mathrm{Im}\P(hp,\omega) \approx (\Sigma |(c_h)_{s'o}|^2)\frac{\pi}{D_s}|\overline{(c_p^+)_{so}}|^2 \quad \varepsilon_s = -(\lambda-\varepsilon_h)-\omega + (\Sigma |(c_p^+)_{so}|^2)\frac{\pi}{D_s}|\overline{(c_h)_{s'o}}|^2 \quad \varepsilon_{s'} = -(\varepsilon_p-\lambda)-\omega \tag{B5}$$

Since the sums in Eq. (B4) are approximately unity, it may be rewritten as

$$\mathrm{Im}\P(hp,\omega) \approx \frac{\pi}{D_s}|\overline{(c_p^+)_{so}}|^2 \varepsilon_s = -(\lambda-\varepsilon_h)-\omega + \frac{\pi}{D_{s'}}|\overline{(c_h)_{s'o}}|^2 \quad \varepsilon_{s'} = -(\varepsilon_p-\lambda)-\omega \tag{B6}$$

Consequently, the argument of W_p, i.e. $\varepsilon_s+\lambda$, must be evaluated at the important value of $\varepsilon_s = -(\lambda-\varepsilon_h)-\omega$. and the argument $(\lambda-\varepsilon_{s'})$ of W_h, must be evaluated at the important value of $\varepsilon_{s'} = -(\varepsilon_p-\lambda)-\omega$. If we make the further

approximation of using these values of ε_s and $\varepsilon_{s'}$ for <u>all</u> excitation energies - i.e. for any separation between the two peaks, not only for the case when the tails are overlapping, the $|\overline{(c_p^+)_{so}}|^2$ and $|\overline{(c_h)_{s'o}}|^2$ become

$$\frac{\pi}{D_s}|\overline{(c_p^+)_{so}}|^2 = \frac{W_p(\varepsilon_h-\omega)}{(\varepsilon_s-\varepsilon_p+\lambda)^2 + W_p^2(\varepsilon_h-\omega)}$$

$$\frac{\pi}{D_{s'}}|\overline{(c_h)_{s'o}}|^2 = \frac{W_h(\varepsilon_p+\omega)}{(\varepsilon_{s'}+\varepsilon_h-\lambda)^2 + W_h^2(\varepsilon_p+\omega)} \qquad \text{(B7)}$$

These two expressions differ from those of Eq.(2.29) in that neither vanish at zero excitation energy. (Previously, at zero excitation energy, we had $W(\lambda)=0$, see Eq.(2.29)). Furthermore, they no longer satisfy the sum rule. However, if $|\overline{(c_p^+)_{so}}|^2$ and $|\overline{(c_h)_{s'o}}|^2$ are sharply peaked, we may recover the sum rule by approximating the sum as an integral, and extending the limits of integration to $-\infty$. Thus the sum rule is satisfied in the approximate sense that

$$\frac{1}{D_s}\int_{\bullet}^{\infty} d\varepsilon_s |\overline{(c_p^+)_{so}}|^2 = \frac{1}{D_{s'}}\int_{\bullet}^{\infty} d\varepsilon_{s'} |\overline{(c_h)_{s'o}}|^2 = 1 \qquad \text{(B8)}$$

We are now in a position to evaluate Eq.(B1). We approximate the sums by the appropriate integrals, and we insert

the expressions for $|\overline{(c_p^+)_{so}}|^2$ and $|\overline{(c_h)_{s'o}}|^2$. Since the ε_s and $\varepsilon_{s'}$ dependence has been removed by this technique of evaluation at the most important values at which they occur, the integral over ε_s and $\varepsilon_{s'}$ may be done, to yield finally,

$$\P(hp,\omega) = [\varepsilon_p - \varepsilon_h - i\{W_h(\varepsilon_p+\omega) + W_p(\varepsilon_h-\omega)+\omega\}]^{-1} \qquad \text{(B9)}$$

The similar results obtained in the evaluation of $\P(ph,\omega)$ were derived using the same technique. [Do 74].

The Pairing Model - A Review.

The standard procedure employed for investigating the consequences of a pairing interaction between nucleons is via the Bogoliubov transformation [Ki 60], defined in Sec.3.1, as

$$A_\alpha^+ = u_a c_\alpha^+ - v_a S_\alpha c_{-\alpha}$$
$$A_\alpha = u_a c_\alpha - v_a S_\alpha c_{-\alpha}^+ \qquad \text{(C1)}$$

where the notation $\pm\alpha=\{a,\pm m_\alpha\}$ and $S_\alpha=(-)^{j_\alpha-m_\alpha}$ was introduced. The quasiparticle creation and destruction operators satisfy the fermion commutation relation $\{A_\alpha,A_\alpha^+\}=\delta_{\alpha\alpha'}$, (i.e. the transformation is canonical), provided that $u_a^2+v_a^2=1$. Inversion of Eq.(C1) is immediate, yielding the relations

$$c_\alpha^+ = u_a A_\alpha^+ + v_a S_\alpha A_{-\alpha}$$
$$c_\alpha = u_a A_\alpha + v_a S_\alpha A_{-\alpha}^+ \qquad \text{(C2)}$$

A complication arises from the transformation (C1), since operations of this nature destroy the conservation of particle number. Thus a Lagrange multiplier λ (the chemical potential) has to be introduced into the many-body Hamiltonian $H'=H-\lambda N=\sum_{\alpha\beta}(T_{\alpha\beta}-\lambda)c_\alpha^+c_\beta-\frac{1}{2}\sum_{\substack{\alpha\beta\\\delta\gamma}}(\alpha\beta|V|\gamma\delta)c_\alpha^+c_\beta^+c_\delta c_\gamma$ to

APPENDIX C.

The Pairing Model - A review.

The standard procedure employed for investigating the consequences of a pairing interaction between nucleons is via the Bogoliubov transformation [Ki 60], defined as ec.3.1, as

$$A^+_\alpha = u_a c^+_\alpha - v_a S_\alpha c_{-\alpha}$$
$$A_\alpha = u_a c_\alpha - v_a S_\alpha c^+_{-\alpha} \qquad (C1)$$

where the notation $\pm\alpha \equiv \{a, \pm m_\alpha\}$ and $S_\alpha = (-)^{j_\alpha - m_\alpha}$ was introduced. The quasiparticle creation and destruction operators satisfy the fermion commutation relation $\{A_\alpha, A^+_\alpha\} = \delta_{\alpha\alpha}$, (i.e. the transformation is canonical), provided that $u_a^2 + v_a^2 = 1$. Inversion of Eq.(C1) is immediate, yielding the relations

$$c^+_\alpha = u_a A^+_\alpha + v_a S_\alpha A_{-\alpha}$$
$$c_\alpha = u_a A_\alpha + v_a S_\alpha A^+_{-\alpha} \qquad (C2)$$

.. complication arises from the transformation (C1), since operations of this nature destroy the conservation of particle number. Thus a Lagrange multiplier λ (the chemical potential) has to be introduced into the many-body Hamiltonian $H' = H - \lambda N = \sum_{\alpha\beta}(T_{\alpha\beta} - \lambda) c^+_\alpha c_\beta - \frac{1}{4}\sum_{\substack{\alpha\beta \\ \delta\gamma}} \langle\alpha\beta|V|\gamma\delta\rangle c^+_\alpha c^+_\beta c_\delta c_\gamma$ to

ensure particle number conservation in the mean. The linear combinations introduced by Eq.(C1) are now employed to effect an approximate diagonalisation of H', in the case that pairing interactions alone are present. The pairing interaction is characterised by two-body matrix elements $\{\alpha\text{-}\alpha|V|\gamma\text{-}\gamma)$ that are only non-vanishing between paired states $\{\alpha,-\alpha\}$ and $\{\gamma,-\gamma\}$. Thus, only pairs of nucleons coupled to J=0 can interact, which in turn necessitates operators of the type given by Eq.(C1) to describe the elementary modes of such a system. Bearing these features in mind, there are now several equivalent methods available [La 64] for obtaining the spectrum of the elementary excitations in the pairing model. One simple way is to linearise the equations of motion for c^+_α and $c_{-\alpha}$. The rate of change of c^+_α is given by $i\dot{c}^+_\alpha = \{c^+_\alpha, H'\}$. Upon linearising, and performing the approximation of pairing (ie $\beta\to-\alpha$, and $\delta\to-\alpha$ in the matrix element of V), this becomes

$$i\dot{c}^+_\alpha = -(\varepsilon_a-\lambda)c^+_\alpha + \sum_\gamma (\alpha\text{-}\alpha|V|\gamma\text{-}\gamma)^* \langle c^+_\gamma c^+_{-\gamma}\rangle c_{-\alpha} \qquad (C3)$$

where the brackets $\langle\ \rangle$ denote the average with respect to the quasiparticle ground state which is yet to be determined. Since $\dot{c}^+_\alpha$ is coupled to $c_{-\alpha}$ by Eq.(C3), we also need the equation for $c_{-\alpha}$. The resulting set of equations can be summarised in matrix form as:

$$i\begin{bmatrix}\dot{c}^{+}_{\alpha}\\ \dot{c}_{-\alpha}\end{bmatrix} = \begin{bmatrix}-(\varepsilon_a-\lambda) & s_\alpha\Delta^{*}_a\\ s_\alpha\Delta_a & E_a-\lambda\end{bmatrix}\begin{bmatrix}c^{+}_{\alpha}\\ c_{-\alpha}\end{bmatrix} \qquad (C4)$$

after introducing the abbreviation $\Delta_a = S_{\alpha\gamma}\langle\alpha-\alpha|V|\gamma-\gamma\rangle\langle c_{-\gamma}c_{\gamma}\rangle$. The Bogoliubov transformation, Eq.(C1) effects the diagonalisation of these equations, showing that the quasiparticle operators, A^{+}_{α} and A_{α}, create and destroy elementary excitations of the interacting system, with excitation energies Λ, given by

$$\begin{vmatrix}-(\varepsilon_a-\lambda)-\Lambda & s_\alpha\Delta_a\\ s_\alpha\Delta_a & (\varepsilon_a-\lambda)-\Lambda\end{vmatrix} = 0 \qquad (C5)$$

$$\text{or } \Lambda=\pm E_a, \quad E_a=\sqrt{(\varepsilon_a-\lambda)^2+\Delta^2_a} \qquad (C6)$$

that reproduces the famous gap equation of Bardeen, Cooper and Schrieffer [Bd 57] . The u_a and v_a then form an eigenvector of the matrix associated with Eq.(C5). One finds from this, using $u_a^2+v_a^2=1$, the relations

$$u^2_a = \tfrac{1}{2}\left[1+\frac{\varepsilon_a-\lambda}{E_a}\right]$$

$$v^2_a = \tfrac{1}{2}\left[1-\frac{\varepsilon_a-\lambda}{E_a}\right] \qquad (C7)$$

expressing the probability that the single hole / particle state is occupied, respectively. The quasiparticle or BCS ground state, $|0\rangle$ acts as a vacuum, for the A^{+}_{α}s,

$$A_\alpha|0\rangle = 0, \qquad \text{(C8)}$$

while $A_\alpha^+|0\rangle$ creates a single quasiparticle of energy E_a above the quasiparticle ground state.

APPENDIX D.

The Hole-vibration Coupling Strength.

The coupling strength f_J used in calculating the coupling of a neutron hole to a proton core vibration also enters into the calculation of effective charge carried by the proton hole in ^{115}In. The self-energy for this state is still given by the expression (3.7) but with the roles of protons and neutrons interchanged. The proton hole is now dressed by a polarisation bubble resulting from the vibration of the valence neutrons. Now pairing is unimportant for the hole line, but important for constructing the polarisation bubble, while damping is unimportant in either component because of the low excitation energy. Hence the self-energy of the proton hole $\bar{p}$ due to its coupling with a collective neutron vibration c becomes

$$\Sigma_{\bar{p}}(\omega) = \frac{|H_{\bar{p}c}|^2}{\omega - \varepsilon_{\bar{p}} - \omega_c} \qquad (D1)$$

where

$$|H_{\bar{p}c}| = \sqrt{\left(\frac{2J+1}{2j_p+1}\right)}\ f_J |Q^J_{\bar{p}\bar{p}}|\,|\Lambda_c| \qquad (D2)$$

see equations (3.7) and (3.21), if as here the proton hole does not change its state during the dressing operation. Since pairing effects are present, the

value given by Eq.(3.16) is replaced by

$$|\Lambda_c|^2 = \left\{ 2f_J^2 \omega_c \sum_{a>b} \frac{(u_a v_b + u_b v_a)(E_a + E_b)(Q^J_{ab})^2}{[(E_a+E_b)^2 - \omega_c^2]^2} \right\}^{-1} \qquad \text{(D3)}$$

when pairing, and the non-degeneracy of the two quasi-particle excitations, E_a+E_b, is recognised. We now use the associated eigenvalue equation [Ba 60]

$$2f_J \sum_{a>b} (u_a v_b + u_b v_a)(Q^J_{ab})^2 \frac{E_a+E_b}{(E_a+E_b)^2-\omega_c^2} = 1 \qquad \text{(D4)}$$

for ω_c to determine $f_{J=2}$ if ω_c=1.27 MeV. The sums in equations (D3) and (D4) run over all pairs of valence neutron states in Table 3.1 that can couple to $J=2^+$. Isolating these and filling in the values of v_a and $u_a=\sqrt{1-v_a^2}$ as well as the associated quasiparticle energies E_a listed there, one finds that ω_c=1.27 MeV is the lowest root of Eq.(D4), provided that f_J=2.04 MeV. The corresponding value of $|\Lambda_c|$ for ω_c=1.27 MeV is $|\Lambda_c|$=1.02. Using this information to calculate $|H_{\bar{p}c}|$ for J=2 and $j_{\bar{p}}$=9/2, one finds that

$$|H_{\bar{p}c}| \cong \sqrt{\frac{5}{10}}\,(2.04)(0.44)(1.02) = 0.65 \text{ MeV} \qquad \text{(D5)}$$

after appealing to the (3.13) and Tables of 3j-symbols [Ed 60] to compute

$$|Q^J_{\bar{p}p}| = \frac{10}{\sqrt{4\pi}} \begin{pmatrix} 9/2 & 9/2 & 2 \\ 1/2 & -1/2 & 0 \end{pmatrix} = \frac{10}{\sqrt{4\pi}}\sqrt{\frac{4}{165}} = 0.44$$

for $j_4=j_3=9/2$.

We may compare Eq.(D5) with the Bohr-Mottelson estimate

$$|H_{\bar{p}c}| \approx \langle j|r\frac{\partial V}{\partial r}|j\rangle\left[(2\lambda+1)\hbar\omega_\lambda/8\pi C_\lambda\right]^{\frac{1}{2}}(j\ \tfrac{1}{2}\ \lambda\ 0\ |\ j\ \tfrac{1}{2})$$

for coupling [Bo 75] a surface phonon λ to a shell model state j. For ^{116}Sn, for which $\hbar\omega_\lambda$=1.27 MeV, and the stiffness parameter C_λ=253 MeV for λ=2, one finds $|H_{\bar{p}c}|\approx$0.8 MeV for j=9/2, if we take the typical value $\langle j|r\frac{\partial V}{\partial r}|j\rangle\approx$50 MeV. The close agreement between these two estimates of $|H_{\bar{p}c}|$, the latter of which gives the correct polarisation charge for ^{115}In (see p 533 of [Bo 75]), is an additional confirmation of the physical validity of the doorway model.

REFERENCES

Ba 60 — M. Baranger, Phys. Rev. 120 (1960) 957

Bd 57 — J. Bardeen, L.N. Cooper and J.R. Schrieffer, Phys. Rev. 106 (1957) 162

Be 69 — Advances in Nuclear Physics, edited by M. Baranger and A. Vogt, (Plenum Press, N.Y) 1969

Bo 75 — A. Bohr and B.R. Mottelson, Nuclear Structure (Benjamin, Reading, 1975), Vol II

Br 72 — G.E. Brown, Many-body Problems, (North Holland, 1972)

Bs 77 — D.R. Bès, Proceedings of the International School of Physics, Enrico Fermi, edited by A. Bohr and R.A Broglia, (North Holland, 1977), page 55.

Ču 63 — B. Čujec, Phys. Rev. 131 (1963) 735

Do 72 — C.B. Dover, R.H. Lemmer, and F.J.W. Hahne Ann. Phys. 70 (1972) 458

Ed 60 — Angular Momentum in Quantum Mechanics, (Princeton University Press, 2nd ed. 1960)

Fe 71 — A.L. Fetter and J.D. Walecka, Quantum Theory in Many-Particle Systems, (McGraw-Hill, N.Y., 1971)

Fs 54 — H. Feshbach, C.E. Porter and V.F. Weisskopf, Phys. Rev. 96 (1954) 448

Fs 58 H. Feshbach, Ann. Phys. (N.Y.) 5 (1958) 357, ibid. Ann. Phys. (N.Y.) 19 (1962) 278.

Fs 67 H. Feshbach, A.K.Kerman and R.H.Lemmer, Ann. Phys. 41 (1967) 230.

Ge 80 E. Gerlic, G. Berrier-Ronsin, G. Duhamel, S. Galès, E. Hourani, H. Langevin-Joliot, M. Vergnes and J. van de Wiele, Phys. Rev. C 21 (1980) 124

Ha 75 F.J.W.Hahne and W.D.Heiss, Ann. Phys. 89 (1975) 68

Ki 60 L.S.Kisslinger and R.A.Sorensen Kgl. Danske Videnskab. Selskab. Mat. Fys. Medd., 32 No 9 (1960)

Kl 82 S.P.Klevansky and R.H.Lemmer, Phys. Rev. C (1982) to be published

La 62 A.M.Lane and J.M.Soper, Nucl. Phys. 37 (1962) 663

La 64 A.M.Lane, Nuclear Theory, (Benjamin, N.Y. 1964)

Ma 76 R.D.Mattuck, A Guide to Feynman diagrams in the Many-Body Problem, (McGraw-Hill, 1976)

My 57 M.G.Mayer and J.H.D.Jensen, Elementary Theory of Nuclear Shell Structure (Wiley 1957)

Pi 66 D. Pines and P. Nozières, The Theory of Quantum Liquids, (Benjamin, N.Y., 1966)

Th 61 D.J. Thouless, Nucl. Phys. 22 (1961) 78

Ul 64 I. Ulehla, G. Ladislav, Z. Pluhar, Optical Model of the Atomic Nucleus. (Academic Press, N.Y. and London, 1964)

Va 74 S.Y. van der Werf, B.R. Kooistra, W.H.A. Hesselink, F. Iachello, L.W. Put, and R.H. Siemssen, Phys. Rev. Lett. 33 (1974) 712

Va 77 S.Y. van der Werf, M.N. Harakeh, L.W. Put, O. Scholten, R.H. Siemssen, Nucl. Phys. A289 (1977) 141

Vo 79 Microscopic Optical Potentials, edited by H.V von Geramb (Springer, Heidelberg 1979), Vol. 89

We 69 J. Weneser, Phys. Rev. 188 (1969) 1747